

Sensitivity of marine heatwaves metrics to SST products, focusing on the Tropical Pacific.

Carla Chevillard¹, Romain Le Gendre^{2,3}, Christophe Menkes⁴, Takeshi Izumo⁵, Bastien Pagli⁵, Simon Van Wynsberge¹ and Sophie Cravatte³

¹Ifremer, UMR 241 SECOPOL (Ifremer, IRD, ILM, UPF), Vairao, Tahiti, French Polynesia

²Ifremer, UMR 9220 ENTROPIE (Institut de Recherche pour le Développement, Université de la Réunion, Ifremer, CNRS, Université de la Nouvelle-Calédonie), Nouméa, New Caledonia.

³Université de Toulouse, LEGOS (IRD, CNES, CNRS, UT3), Toulouse, France.

⁴IRD, UMR 9220 ENTROPIE (Institut de Recherche pour le Développement, Ifremer, Université de la Réunion, Université de la Nouvelle-Calédonie), Nouméa, New Caledonia

⁵IRD, UMR 241 SECOPOL (Ifremer, IRD, ILM, UPF), Faa'a, Tahiti, French Polynesia

Correspondence to: Carla Chevillard (carla.chevillard@ifremer.fr)

Abstract. Marine heatwaves (MHWs) are increasingly studied in climate sciences for their ecological impacts, for which accurate real-time bulletins and forecasts are essential. Yet, methodological choices in their detection affect metric estimates, underlining the need to better assess these sensitivities. This study provides a thorough assessment of the impact of ~~s~~Sea ~~t~~Surface ~~t~~emperature (SST) product choice on MHW statistics, focusing on the tropical Pacific. MHW detection was performed on six daily gridded SST datasets: four widely used blended satellite observational products, one ocean reanalysis, and a multi-dataset ensemble mean computed from the four observational products. Sensitivity to SST products was evaluated for six MHW metrics (MHW days per year, number of events per year, duration, maximum intensity, cumulative intensity and onset rate) and for the ~~d~~Degree ~~h~~Heating ~~w~~Weeks (DHW), a widely used ~~index~~proxy for coral bleaching ~~risk~~. Inter-product comparisons revealed a significant dispersion among MHW metric estimates, ~~with~~ ~~t~~The reanalysis GLORYS12v1 ~~detected~~~~detecting~~ fewer, longer and less intense MHWs while OISST detected more MHWs of shorter duration and higher intensity, ~~likely~~ related to their ~~respectively~~ weak and strong high-frequency SST variability (periods shorter than 2 weeks) ~~of the two products~~~~respectively~~. The sensitivity analysis showed that the onset rate was the most sensitive metric to SST product choice and the maximum intensity the most robust ~~one~~. Metrics uncertainties were quantified inside seven regions of the basin and were largest in the western Pacific Warm Pool. Co-occurrence analyses of MHWs revealed that, over the basin, 10 to 80% of MHW days were detected simultaneously by all products, with the western Pacific Warm Pool showing the lowest agreement (10–40%). Filtering MHWs by size also revealed that the detection of large-scale MHWs ($> 5^\circ\text{lon} \times 5^\circ\text{lat}$) was more consistent across products than smaller ~~scale~~ ones. Finally, over the studied period, inter-product differences tended ~~ed~~ to decrease with time. The DHW also revealed to be sensitive to SST products, with inter-product differences on DHW annual maximum reaching more than $1^\circ\text{C}\cdot\text{weeks}^{-1}$ and percentages of bleaching alert days ($\text{DHW} \geq 4^\circ\text{C}\cdot\text{weeks}^{-1}$) in common across products reaching 70% at most across much of the basin. These findings contribute to a better understanding of how ~~SST~~ ~~product choice~~~~methodological choices~~ affects the characterization of MHWs and DHW, and their associated uncertainties.

34 1- Introduction

35 Between April 2023 and July 2024, global ocean surface temperatures reached their highest level ever registered (Terhaar et
36 al., 2025). These extremes observed in global mean ~~s~~Sea ~~s~~Surface ~~t~~Temperatures (SST), partly related to an El Niño event,
37 would not have been reached without the acceleration of ocean warming over the last decades (Merchant et al., 2025). They
38 manifest locally as “marine heatwaves” (MHWs), a term first introduced by Pearce et al. (2011). Hobday et al. (2016) further
39 formalized the definition of a MHW as an episode of temperatures above a climatological threshold for at least five consecutive
40 days, characterized by its duration, intensity, rate of evolution and spatial extent. Due to their significant ecological and
41 biological impacts (Capotondi et al., 2024), MHWs have become a hot topic in ocean science, more so as climate models
42 predict significant increases in their frequency, intensity and duration due to global warming (Frölicher et al., 2018; Oliver et
43 al., 2019).

44 Real-time MHW information and forecasts are of crucial interest to managers and stakeholders as they support marine
45 conservation and fisheries management (Holbrook et al., 2020; Hartog et al., 2023; Hobday et al., 2023; Kajtar et al., 2024;
46 Spillman et al., 2025). Such bulletins must provide accurate information, ideally combined with uncertainty estimates.
47 Explicitly accounting for the methodological choices in MHW detection (Farchadi et al., 2025), and, consequently, quantifying
48 the associated uncertainties, are key to MHW research and to assess their socio-ecological impacts.

49 MHW detection ~~requires~~~~implies~~ several methodological choices: the choice of the SST product, the ~~definition~~~~length~~ of the
50 climatological baseline, whether or not to detrend the SST time series, and the definition of the MHW threshold (Farchadi et
51 al., 2025). ~~If the scientific community agrees on the general methodology—use of 30-year climatology, no detrending and~~
52 ~~seasonally varying 90th percentile, Hobday et al., 2016—different~~ For better agreement across studies, the scientific community
53 ~~agrees on a common methodology (use of 30-year climatology, no detrending and seasonally varying 90th percentile, Hobday~~
54 ~~et al., 2016) even though other~~ options can lead to significantly different results in MHW metrics evaluation potentially leading
55 to different policy responses to MHWs (Capotondi et al., 2024).

56 While the effects ~~of the choice~~ of the climatological baseline ~~choice~~ (Amaya et al., 2023), of detrending (Smith et al., 2025)
57 and of the use of a fixed threshold (Langlais et al., 2017) have been investigated and discussed, the impact of SST product
58 choice on MHW detection statistics remains little explored. ~~T~~~~h~~~~i~~~~s~~ step appears crucial for MHW analysis (Farchadi et al.,
59 2025), ~~yet~~ most MHW studies rely on a single blended SST product, either satellite-only or satellite combined with in situ
60 data, or an ocean reanalysis. A similar issue applies to the ~~d~~Degree ~~h~~Heating ~~w~~Weeks (DHW) computation, a widely-used
61 metric for coral bleaching risk that represents accumulated heat stress which can lead to coral bleaching and mortality (Skirving
62 et al., 2020). This metric is also computed from a single SST product in most coral studies. Yet, SST products differ in their
63 data sources, processing and interpolation methods, and they consequently ~~exhibit differences~~~~show variability between~~
64 ~~themselves~~ (Martin et al., 2012; Dash et al., 2012; Okuro et al., 2014).

65 Several studies have focused on intercomparing satellite-derived SST products, particularly with regard to trends (Menemenlis
66 et al., 2025) or through validations using in-situ observations (Fiedler et al., 2019). Nevertheless, while some studies have

67 shown that MHW characteristics can be biased depending on the chosen SST product (Wang et al., 2024; Lal et al., 2025), the
68 sensitivity of MHW metrics to the choice of SST product has been scarcely investigated, and to our knowledge, has never been
69 quantified at global or ~~basin-wide~~regional scales. Marin et al. (2021) identified locations where significant differences between
70 products occur, but for coastal MHWs. For DHW, several studies showed significant differences between datasets in specific
71 areas (for instance, Neo et al. 2023 compared four datasets in the North Western and South Western Australian reefs;
72 Margaritis et al. 2025 compared two datasets in the Caribbean).

73 Such quantification would help ~~improving to improve~~ the consistency of MHW information ~~and forecasts~~, which is crucial in
74 basins like the tropical Pacific where communities heavily rely on marine resources (Holbrook et al., 2022; Lal et al., 2025).
75 In this large zone (almost half of the tropics), MHWs are modulated by El Niño Southern Oscillation (ENSO) (Holbrook et
76 al., 2019; Sen Gupta et al., 2020; Pagli et al., 2025), although other phenomena, such as the Madden Julian Oscillation (MJO)
77 (Madden and Julian 1971,1972) and tropical cyclones, can also influence MHW life cycle (Dutheil et al., 2024). There,
78 societies and environments are particularly vulnerable to MHWs (Andréfouët et al., 2015; Smith et al., 2021, 2024), making
79 the tropical Pacific an area of strong interest to MHW research.

80 The present study consequently provides a quantitative assessment of the sensitivity of MHW metrics to ~~SST product choice~~the
81 ~~choice of the SST product~~, focusing on the tropical Pacific. Six SST datasets are compared: four blended multi-satellite
82 observational products, one ocean model reanalysis product, and an ensemble-mean product computed as the average of the
83 four SST observational products. Six MHW metrics (number of MHW days per year, number of events per year, duration,
84 maximum intensity, cumulative intensity and onset rate) ~~were~~are analyzed to determine which metrics are more robust to SST
85 product choice. In addition, the sensitivity of DHW index to SST products ~~was assessed~~is assessed for the DHW index. A
86 regional approach ~~was~~is also conducted by dividing the tropical Pacific into seven regions and providing spatially averaged
87 uncertainties for MHW metrics and DHW inside these regions, in line with the recommendations of Farchadi et al. (2025) who
88 highlight the importance of accounting for regional variability in MHW studies.

89 The present study is organized as follows. Section 2 describes the data and methodology. Section 3 first provides a comparison
90 of MHW metrics across SST products revealing the impact of high frequency SST variability on MHW detection. A
91 quantitative assessment of the uncertainty associated with the SST product choice is then conducted for each metric at both
92 basin and regional scales, highlighting the highest sensitivity in the western Pacific Warm Pool. Lastly, similar analysis and
93 evaluation of DHW uncertainties linked to the SST choices is also performed. Finally, the results are discussed in section 4.

94 **2- Data and methodology**

95 **2.1- SST products**

96 ~~In this study, Six SST datasets were used in the study:~~ four observation-based products, their ensemble-mean, and one ocean
97 model reanalysis ~~were analysed~~. We used four daily global L4 (Level 4, gap-free, gridded) SST analysis products : the NOAA
98 Advanced very High Resolution Radiometer (AVHRR) Optimum Interpolation (OI) ¼ degree daily SST v2.0 Analysis data

99 (hereafter designed as OISST), the ESA C3S global Sea Surface and Sea Ice Temperature Reprocessed product (hereafter
100 designed as C3S), the global ocean OSTIA SST and Sea Ice reprocessed product, and the NOAA Coral Reef Watch (CRW)
101 version 3.1 daily global 5km SST product known as CoralTemp. These products are among the most commonly used in MHW
102 studies. We also used the ocean reanalysis GLORYS12v1 as: 1) reanalyses are widely used in MHW research to better
103 understand MHW vertical extent and driving mechanisms (Capotondi et al., 2024; Dutheil et al., 2024), 2) this reanalysis is
104 also used for MHW reports/forecasts by Mercator-Ocean for Copernicus Marine Service¹. The GLORYS12v1 reanalysis used
105 here is a 1/12° reanalysis using the NEMO (Nucleus for European Modelling of the Ocean, Madec et al., 2024) ocean model,
106 forced by ECMWF ERA-Interim atmospheric reanalysis (Dee et al, 2011), complemented by ERA5 re-analyses (Hersbach et
107 al., 2020) for recent years (from January 1st 2019). This reanalysis assimilates sea level anomalies (SLA), observed SST
108 (OISST), sea ice concentration and in situ temperature and salinity vertical profiles (Lellouche et al., 2021).
109 For MHW inter-comparison, C3S, OSTIA, CRW and GLORYS12v1 were regridded on the OISST 0.25° grid using the
110 conservative method “remapcon” from CDO software (Schulzweida et al., 2023). Finally, a sixth dataset hereafter referred to
111 as “COMPOSITE”, was constructed to evaluate the relevance of a multi-product approach for MHW analysis. More precisely,
112 the daily 0.25° COMPOSITE was computed as the mean of the four SST observation-based products: the three re-gridded
113 C3S, CRW and OSTIA, and the raw OISST. The reanalysis GLORYS12v1 was not included in the COMPOSITE since it
114 differs by definition from observation-based products. MHW detection was thus performed on these six 0.25° daily datasets.
115 A summary of information for these datasets is provided in Table 1.

116
117

Table 1: Description of the SST datasets.

Product Reference	Time coverage and temporal resolution	Spatial resolution	Depth	Description and data sources
C3S E.U. Copernicus Marine Service Information (CMEMS). Marine Data Store (MDS) doi:10.48670/moi-00169	31/08/1981-30/12/2024 Daily	0.05°x0.05°	Representative of the 20cm depth.	Reprocessed SST analysis using temperature from satellites: L3U (A)ATSR, SLSTR, AVHRR, AMSR-E, AMSR-2 v3.0 of ESA SST_cci CRD and ICDR and EOCIS. It is independent from in-situ data.
Coral Temp NOAA Coral Reef Watch (CRW) Skirving et al., 2020	01/01/1985-present Daily	0.05°x0.05°	Representative of the 20cm depth.	Reprocessed SST analysis derived using a combination of 3 L4 nighttime-only satellite SST datasets (two NOAA Geo Polar SST products - Near Real Time and reprocessed - and the 1985-2002 daily global nighttime only foundation SST from OSTIA).

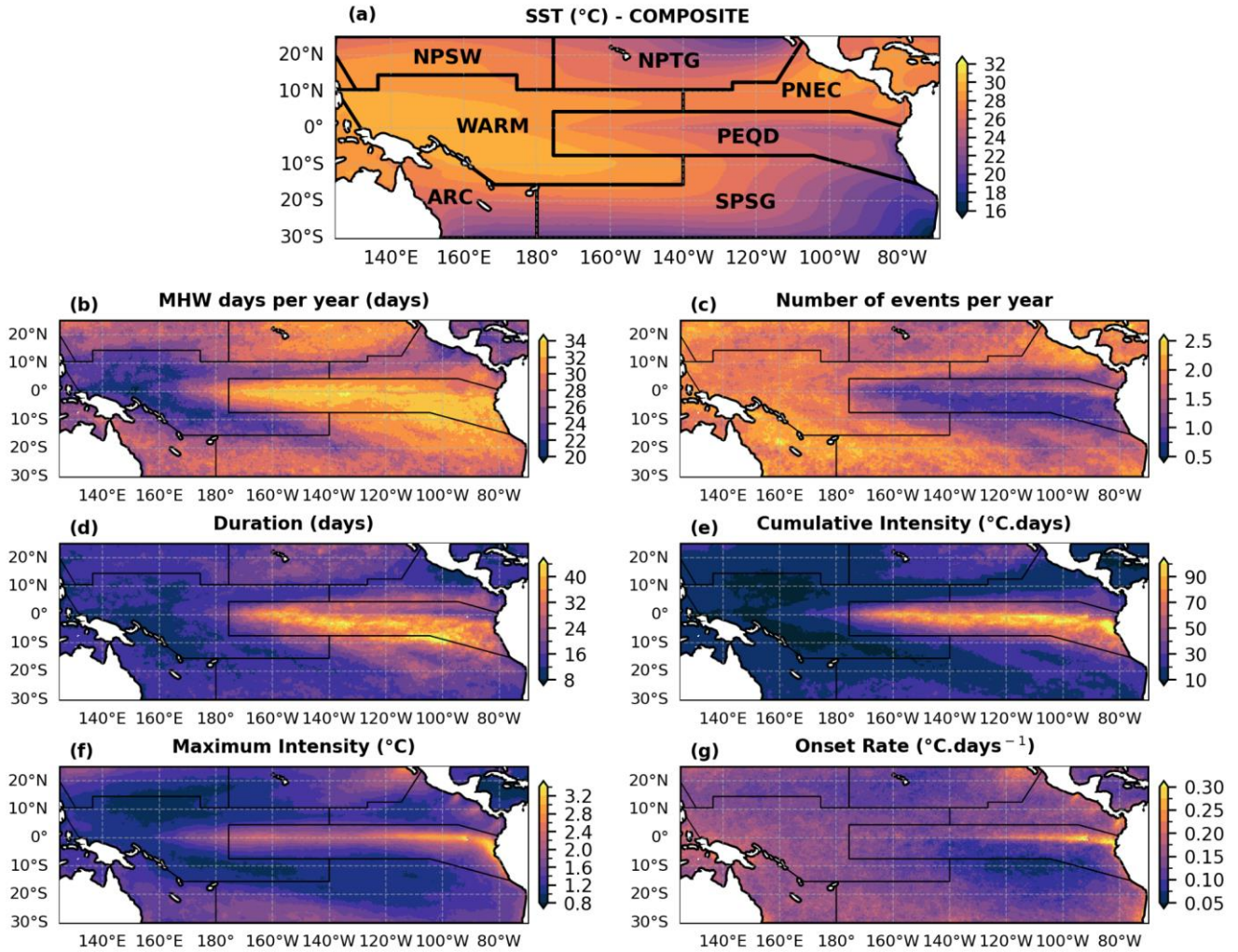
¹ <https://www.mercator-ocean.eu/ocean-intelligence/ocean-bulletins-and-insights/marine-heatwaves-archive/>

<u>OSTIA</u> E.U CMEMS. MDS doi:10.48670/moi-00168	30/09/1981 - 31/05/2022 Daily	0.05°x0.05°	SST foundation i.e. SST free of diurnal variability. This is very similar to the temperature measured nominally at a depth of 0.2-1m just before sunrise (Donlon et al., 2012)	Reprocessed SST analysis using satellite data (re-processed ESA SST CCI, C3S [RD.2] EUMETSAT and REMSS) and in-situ data from the HadIOD dataset (ships and buoys).
<u>OISSTv2</u> NOAA Reynolds et al., 2007 Huang et al., 2021	01/09/1981 - present Daily	0.25°x0.25°	Representative of the 20cm depth.	Reprocessed SST analysis using satellite data (AMSR, AVHRR and AVHRR-Only) and in-situ data from ships, buoys and Argo floats.
<u>GLORYS12v1</u> E.U CMEMS. MDS doi:10.48670/moi-00021	31/12/1992 - 26/05/2025 Daily	0.08x0.08°	0.49m (minimum depth of the 50 vertical levels)	Ocean reanalysis. Assimilated temperature observations : OISST (Reynolds 0.25° AVHRR-only SST), in situ temperature profiles from Copernicus Marine CORAv4.1 database.
<u>COMPOSITE</u>	01/01/1993-31/12/2021	0.25°x0.25°	-	Mean of the four SST analysis products, <u>having regridded C3S, CRW and OSTIA to the OISST 0.25° grid. - C3S, CRW and OSTIA all three re-gridded at 0.25°, and OISST.</u>

119 2.2- MHW and DHW analyses

120 2.2.1- Study area

121 MHW and DHW analyses were performed over the tropical Pacific (30°S - 25°N; 125°E - 70°W, Fig. 1A) at 0.25° spatial
122 resolution. The latitudinal coverage is not symmetric with respect to the equator, extending further south to include islands of
123 the southern subtropical Pacific, notably French Polynesia (30°S - 0°S; 165°W - 130°W). As MHW characteristics and ocean
124 processes vary within this area (Holbrook et al., 2019, 2022; Lal et al., 2025), the sensitivity analysis was conducted detailed
125 at regional scale for both MHW metrics and DHW. Seven regions were defined based on the Longhurst et al. (2007) provinces
126 which reflect different “eco-regions” functioning with specific the ocean’s physical and biogeochemical ocean properties. As
127 will be shown later, these regions also correspond to areas with distinct MHW characteristics, and represent different physical
128 regimes in the tropical Pacific. Results of the basin-scale sensitivity analysis were thus aggregated within these regions. These
129 regions are drawn ~~They are illustrated~~ in Fig. 1a and named following Longhurst et al. (2007): the North Pacific Subtropical
130 Gyre West (NPSW), North Pacific Tropical Gyre (NPTG), West Pacific Warm Pool (WARM), North Pacific Equatorial
131 Countercurrent (PNEC), Pacific Equatorial Divergence (PEQD), Archipelagic Deep Basins (ARC) and the South Pacific
132 Subtropical Gyre Province (SPSG) (Fig. 1a). Minor adjustments were made to the original WARM province of Longhurst et
133 al. (2007), with a small extension further east at the borders with the PNEC and SPSG, to better capture the coherent dispersion
134 patterns of MHW metrics.



135

136

137

Figure 1: (a) Mean SST (1993-2021) from the COMPOSITE in the tropical Pacific, with the regions of study. (b-g) Ensemble mean of MHW metrics in the tropical Pacific (1993-2021; cf. section 2.3.1), with the limits of the regions defined in (a).

138

2.2.2- MHW and DHW computation

139

MHW detection was performed for each pixel of the six datasets presented in section 2.1 on the 0.25° common grid over the tropical Pacific and the period 1993-2021, following the Hobday et al. (2016) method. A MHW event was defined as a period of at least five consecutive days during which SST exceeded the local 90th percentile threshold. Events separated by fewer than two days were considered as a single continuous event Gaps of less than two days within an event were ignored. The analysis was conducted over 1993-2021, which. The full study period 1993-2021 also served as the common climatological baseline across the SST products (Table 1, common period to all products). No detrending was applied to the SST time series in order to account for differences in long-term SST trends among products (Menemenlis et al., 2025). The sensitivity analysis was

144

145

146 carried out for six MHW metrics: (1) the number of MHW days per year, (2) number of events per year, (3) event duration,
147 (4) maximum intensity, (5) cumulative intensity, and (6) onset rate. The number of MHW days per year and the number of
148 events per year were defined as the total number of days and events over 1993-2021 divided by the 29 years of the analysis
149 period. Maximum and cumulative intensities were expressed relative to climatology, with cumulative intensity calculated as
150 the sum of daily intensities over each event's duration. The onset rate was defined as the rate of temperature increase from the
151 start of a MHW to its maximum intensity (Hobday et al., 2016).

152

153 Daily ~~d~~Degree-~~h~~Heating ~~w~~Weeks (DHW) values were computed following Skirving et al. (2020) for each pixel of the six SST
154 datasets of section 2.1 at 0.25° resolution. First, daily temperature anomalies (HotSpot) were calculated relative to the local
155 Maximum of Monthly Mean (MMM), defined as the maximum of monthly climatological means over 1993-2021. DHW
156 values on a given day were then computed as the sum over the preceding 12 weeks of daily HotSpot anomalies exceeding 1°C.
157 This accumulated sum was divided by 7 to express DHW in °C weeks⁻¹. Due to its ecological relevance, we investigated the
158 impact of SST product choice on the yearly maximum DHW values in the tropical Pacific. More precisely, this metric
159 quantifies the maximum accumulated heat during a year that can potentially stress marine organisms such as corals.

160 2.2.3- Filtering MHWs by size

161 In order to better understand the origin of inter-product differences in MHW metric estimates, MHWs were filtered by size.
162 The sensitivity analysis was carried out for micro (maximum area $\leq 5^\circ \text{lon} \times 5^\circ \text{lat}$) and macro (maximum area $> 5^\circ \text{lon} \times 5^\circ \text{lat}$)
163 events, separately. ~~MHWs spatial extent was characterised as follows: More precisely,~~ for each day, all pixels where MHWs
164 were detected were assigned a MHW area, defined as the number of contiguous pixels to the studied pixel also experiencing a
165 MHW. ~~These joint pixels are connected along either north-south or west-east directions and. These joint pixels~~ were detected
166 thanks to the label function from python package scipy.ndimage (method inspired from Bonino et al., 2023). In a pixel, a
167 MHW was thus associated with a series of areas over its duration. The maximum area reached during the event was associated
168 with each MHW in the evaluated pixel. Events with a maximum area smaller than 25 square degrees ($5^\circ \times 5^\circ$) were classified
169 as micro-scale, whereas those with a maximum area exceeding 25 square degrees were defined as macro-scale (~~Lal et al.,~~
170 ~~2025~~). The threshold of 25 square degrees was chosen as it filters out MHWs linked to large mesoscale eddies and it is in line
171 with other MHW studies (Lal et al., 2025; Sen Gupta et al., 2020; Sun et al., 2023). The distribution of MHW maximum sizes
172 in the Tropical Pacific for all studied products confirmed that this threshold was appropriate for our study (not shown). The
173 4°x4° threshold was also tested and our results remained almost unchanged, showing that our analysis is robust and not highly
174 dependent on the threshold chosen (not shown).
175 However, since our area of study is bounded spatially, the spatial extent of MHWs at the northern and southern frontiers of the
176 tropical Pacific should be considered carefully (as joint pixels can't extend further south and north, respectively). MHWs
177 spatial extent at these frontiers might actually be larger than it appears in our results.

2.2.4- Filtering MHWs according to El Niño Southern Oscillation

Since ENSO is a dominant driver of MHWs in the tropical Pacific (Holbrook et al., 2019; Sen Gupta et al., 2020; Pagli et al., 2025), the dependence of our results on the ENSO phase was explored. For this purpose, MHWs were divided into three groups : El Niño MHWs, La Niña MHWs, and neutral MHWs. El Niño MHWs were defined as MHWs starting during a month where the Oceanic Niño Index (ONI) was higher than 0.5 and La Niña MHWs were defined as MHWs starting during a month where the ONI was lower than -0.5. The monthly timeseries of the ONI used here are available at : <https://psl.noaa.gov/data/timeseries/month/>. All other MHWs were classified in the neutral group.

2.3- Sensitivity analysis

2.3.1- Inter-product differences and uncertainty quantification

Inter-product differences in MHW detection were illustrated by maps of mean MHW metrics for each SST product over the tropical Pacific and the time period (1993-2021). For duration, maximum intensity, cumulative intensity and onset rate, each pixel of these maps was/were defined at each pixel as the mean value across all MHWs detected between 1993 and 2021. For the number of MHW days per year and the number of events per year, the maps were defined at each pixel as in 2.2.2.

To better highlight the inter-product differences on MHW metrics, anomalies were also mapped over the tropical Pacific. For each product and metric, the product anomaly at each pixel was defined as the difference between the metric value for that product (as defined above) and the ensemble mean value of the metric over all the 6 products except the COMPOSITE (i.e. the mean of five six values, hereafter designated as “ensemble mean” metric) (Eq. 1):

$$anomaly(metric_i, product_j, pixel_k) = metric_i(product_j, pixel_k) - ensemble_{mean}(metric_i, pixel_k) \quad (1)$$

where $ensemble_{mean}(metric_i, pixel_k) = (\sum_{j=1}^5 metric_i(product_j, pixel_k)) / 5$, with i varying from 1 to 6 and representing the six evaluated metrics, j varying from 1 to 56 and representing the 56 evaluated products C3S, CRW, OSTIA, OISST and GLORYS12v1, and k representing the pixel number in the domain. The same maps were produced for the temporal mean of DHW annual maxima (section 2.2.2). Mean metrics and anomalies were computed for the COMPOSITE but the latter was removed from the ensemble-based statistics to avoid counting the observational products twice, since the composite is derived from them.

The sensitivity of each MHW metric to SST product choice was evaluated at each pixel by computing the dispersion of the metric across all the six SST products excluding the COMPOSITE (hereafter designated as “ensemble dispersion”, Eq. 2).

$$\sigma = ensemble_{dispersion}(metric_i, pixel_k) = \sqrt{\frac{1}{5} \sum_{j=1}^5 [(metric_i(product_j, pixel_k) - ensemble_{mean}(metric_i, pixel_k))]^2} \quad (2)$$

The ensemble dispersion was also computed for DHW. Maps of dispersion over the tropical Pacific were produced for each metric. These values of ensemble dispersion were defined as the “uncertainty” of the metric with respect to SST product choice. In order to quantify and compare metrics sensitivity, the ensemble dispersion at each pixel was in some instances also expressed

209 as a percentage by dividing the ensemble dispersion by the ensemble mean value of the metric at that pixel, and then
210 multiplying by 100.

211
212 The co-occurrence of MHWs across SST products was also assessed by computing the percentage of common MHW days
213 over the basin. At each pixel, this percentage was defined as the number of days detected simultaneously as a MHW in all ~~six~~
214 products excluding the COMPOSITE divided by the ensemble mean number of total MHW days at that pixel. Similar analysis
215 was conducted for DHW, by computing the percentage of common bleaching alerts of level 1 (days for which
216 $DHW \geq 4^{\circ}C \cdot weeks^{-1}$) across products.

217 2.3.2- Temporal evolution

218 The temporal evolution of MHW metrics sensitivity to SST product choice was evaluated by computing yearly time series of
219 ensemble dispersion for each metric and region. For this purpose, yearly maps of MHW metrics and ensemble dispersion over
220 the tropical Pacific were produced, following the method described in section 2.3.1. The year attribution of a MHW was based
221 on its onsettime-start. Then, spatial averages of these yearly values of ensemble dispersion were computed within each region,
222 to yield one annual dispersion value per metric and region. The spatial average of ensemble dispersion values inside a region
223 was computed for a given year if dispersion values could be computed for at least 10% of the pixels of the region.

224
225 The temporal evolution of metrics sensitivity to SST product choice was also assessed by computing yearly time series of
226 inter-product spatial correlation within all regions (hereafter designated as “ensemble spatial correlation”). For each region
227 and year, spatial correlation between pairs of products was quantified using the uncentered statistic of pattern correlation
228 ~~methods~~ (Barnett and Schlesinger, 1987), which correlates fields without removing the spatial means. The uncentered statistic
229 was used here since IPCC reports argue that it is better suited ~~for detection in pattern correlation studies~~ as it includes the
230 response in the global spatial mean, while the centered statistic is more appropriate for attribution because it better measures
231 the similarity between spatial patterns (IPCC, 2001). The uncentered pattern correlation statistic is defined ~~as in Eq-3:~~

$$232 \text{PatternCorrelation}(\text{product}_a, \text{product}_b) = \frac{\sum_{k=1}^n a_k b_k}{\sqrt{\sum_{k=1}^n a_k^2 \sum_{k=1}^n b_k^2}} \quad (3)$$

233 where n is the pixel number in the region, a and b represent yearly metrics ~~values~~ for two SST products inside the region
234 ~~evaluated (n pixels in the region)~~.

235 The value of pattern correlation was considered significant when the associated p--value (based on student t-test) was less
236 ~~than inferior to~~ 0.01 (e.g. 99% significance). For a given metric, region and year, the pattern correlation was computed for all
237 ~~10+5~~ product pairs (pairs excluding the COMPOSITE), and these ~~10+5~~ values were averaged to give the yearly value of the
238 ensemble spatial correlation in the region studied. The spatial correlation inside a region was computed for a given year if
239 ensemble spatial correlation values could be computed for at least 10% of the pixels of the region.

240 3- Results

241 3.1- MHW characteristics in the Tropical Pacific

242 Ensemble mean MHW metrics over 1993-2021 are shown in Fig. 1 in the tropical Pacific, with patterns reflecting spatial
243 variability associated with ENSO. In the central and eastern Equatorial Pacific (PEQD), El Niño ENSO largely drives MHW
244 risk (Holbrook et al., 2019; Capotondi et al., 2022). Although MHW occurrences are relatively low in this area (Fig. 1c), the
245 number of MHW days per year is highest, exceeding 32-34 days (Fig. 1b). Here, MHWs have longer durations as they last
246 between 30 to more than 50 days on average (Fig. 1d), and exhibit the highest maximum intensity (more than 3.5°C, Fig. 1f)
247 and cumulative intensity (more than 100°C.days, Fig. 1e) (Holbrook et al., 2019; Oliver et al., 2021). The highly intense
248 MHWs observed in a narrow band along the Equator (2°S-2°N) near the South American Coast are also associated with the
249 highest onset rates of the tropical Pacific (more than 0.3°C/days, Fig. 1g).

250 In the Northeastern tropical Pacific (NPTG), MHWs occur on more than 30 days per year (Fig. 1b) but the number of events
251 is low (~ 1 per year, Fig. 1c). These events are relatively long (30 days, Fig. 1d) and intense (cumulative intensity of 40-
252 50°C.days, Fig. 1e). In contrast, the PNEC experiences one of the highest numbers of events (more than 2.5 per year, Fig. 1c,
253 also observed by Holbrook et al., 2019; Oliver et al., 2021). This area, influenced by the North equatorial countercurrent
254 dynamics, is characterized by short (less than 15 days, Fig. 1d) but intense events, with maximum intensity reaching 2.5°C
255 (Fig. 1f). These features are likely linked to the high SST variability of the region, which favors strong MHW intensities
256 (Oliver et al., 2021).

257 In the southwest tropical Pacific (~~mainly ARC~~), MHW occurrence is modulated by La Niña conditions (Sen Gupta et al., 2020;
258 Lal et al., 2025). ~~M~~In the ARC, mesoscale eddies close to the eastern Australian coast (Bian et al., 2023; Chapman et al., 2025)
259 along with downwelling Rossby waves and downwelling-favourable winds also favor MHW development (Misra et al., 2021;
260 Li et al., 2023; Lal et al. 2025). In this region, MHWs are relatively frequent (more than 2 events per year, Fig. 1c) but short
261 (less than 15 days Fig. 1d, Holbrook et al., 2019). Both the number of MHW days and the maximum intensities are close to
262 the tropical Pacific average (around 25 days and 1.5°C, respectively, Fig. 1b,f). Similar MHW characteristics are observed in
263 the western SPSG and in NPSW. The Northeastern part of the SPSG close to the PEQD is rather influenced by ENSO, with
264 fewer MHWs of longer duration and lower onset rate. The shortest MHWs (less than 10 days, Fig. 1d) are observed in the
265 WARM region. Here, the number of MHW days per year, as well as the cumulative and maximum intensities reach their
266 lowest levels in the tropical Pacific (~15 days per year, <10°C.days and 1°C, respectively). Nevertheless, this region records
267 a high number of events with more than 2.5 events per year close to Papua New Guinea and eastern Indonesian coasts~~the~~
268 Indonesian coast (Fig. 1c, also observed in Holbrook et al., 2019; Oliver et al., 2021).

269 3.2- Inter-product comparison and ranking

270 The MHW analysis performed over the six SST datasets reveals significant differences across products, as illustrated by the
271 MHW days per year computed for each product (Fig. 2a-f). The associated maps of anomalies (Fig. 2g-l; section 2.3.1) allow
272 us to more easily identify potential outliers. Figures S1-S5 extend the inter-product comparison to the other metrics.
273 If the main spatial patterns of mean MHW metrics described in section 3.1 are common between all products, Fig. 2 and Fig.
274 S1-S5 highlight that values can differ by almost a factor of two between products. For the MHW days per year (Fig. 2a-f), the
275 largest differences are observed in the WARM region, with GLORYS12v1 detecting 30 MHW days per year while OISST
276 detects around 15 days per year. Anomalies relative to the ensemble mean range approximately between ± 5 days per year
277 inside the tropical Pacific, with some areas showing even larger anomalies (Fig. 2g-l). The strongest positive (negative)
278 anomalies are observed for GLORYS12v1 (OISST). GLORYS12v1 systematically detects more MHW days than the other
279 products, and OISST less MHW days. C3S and OSTIA show smaller anomalies for this metric. For all products, anomalies
280 are closer to zero in the PEQD, a region of strong influence of ENSO where the longest MHWs are observed (section 3.1).
281 For the other metrics, anomalies generally remain within ± 0.5 events per year, ± 10 days for MHW duration, $\pm 0.25^\circ\text{C}$ for
282 maximum intensity, $\pm 15^\circ\text{C}\cdot\text{days}$ for cumulative intensity and $\pm 0.15^\circ\text{C}/\text{days}$ for onset rate over the tropical Pacific
283 (Supplementary Fig S1-S5). As for the MHW days per year, anomalies for the other metrics reveal that GLORYS12v1 and
284 OISST show the largest anomalies, whereas C3S, CRW and OSTIA are closer to the ensemble mean - except near [Papua New](#)
285 [Guinea and eastern Indonesia](#)~~-the Indonesian coast~~ where OSTIA shows strong positive anomalies in event frequency and
286 onset rate. Unlike the number of MHW days per year, anomalies for other metrics vary substantially in space, and can be either
287 positive or negative within the tropical Pacific for the same product (especially for the number of events per year).

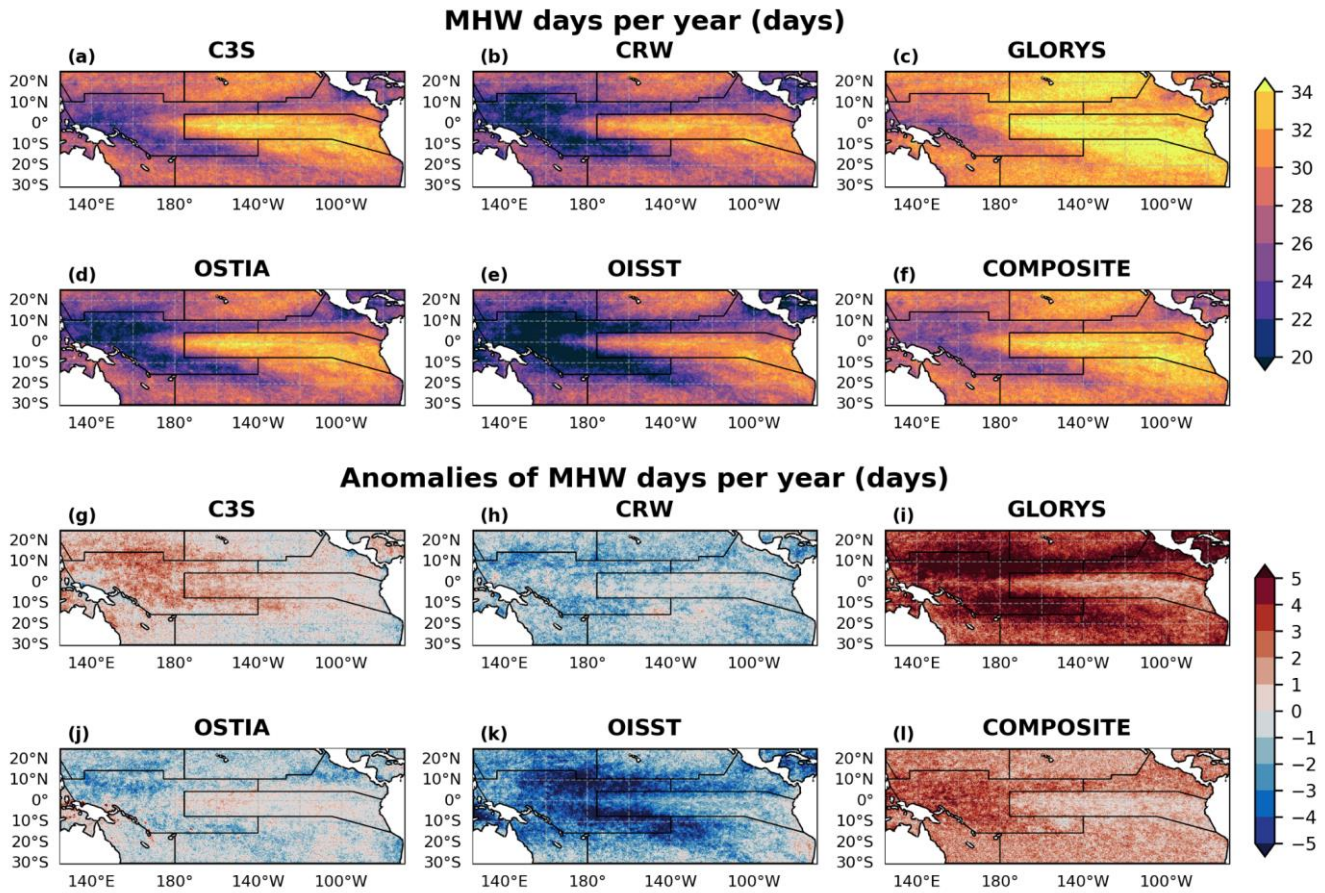


Figure 2: (a-f) Number of MHW days per year over the period 1993-2021 for the six SST products. (g-l) Anomalies of MHW days per year for each product relative to the ensemble mean (section 2.3.1). Black lines indicate regions' limits.

To summarize inter-product differences, the average of MHW metrics for all events detected in the whole domain-tropical Pacific over during 1993-2021 were computed for each product (Fig. 3). For a given metric, the minima and maxima across products of these average values were defined so that values on Fig. 3 represent the average value of the given product minus the minimum across products, divided by the difference between maximum and minimum. This normalization standardizes the results between 0 (product ranking last) and 1 (product ranking first) allowing an easier comparison between products. The distance to the center also gives the information on whether the averaged values of some products are closer to others and if some products behave differently. In the study area, OISST ranks first for maximum intensity, onset rate, and the number of events detected (Fig. 3). By “ranking”, we only mean to compare products but not to determine if one performs better than another. Conversely, OISST shows the lowest ranking for the number of MHW days, duration and cumulative intensity (Fig. 3). The opposite pattern is observed for GLORYS12v1 reanalysis which shows the highest ranking for duration, cumulative intensity and the number of MHW days detected, while it ranks last for MHW maximum intensity and onset rate. The

COMPOSITE product tends to show a similar radar shape as follow the rankings of GLORYS12v1, with radar charts showing similar shapes (Fig. 3). OISST and GLORYS12v1 also therefore stand out in this study, consistently occupying either the lowest or highest ranks across MHW metric estimates even if their variable ranking differs in a complementary manner. By contrast, C3S shows a more “balanced” radar chart, with no clear overestimation or underestimation compared to other products. These findings are consistent with the anomaly analysis presented in Fig. 2 and Fig. S1-S5.

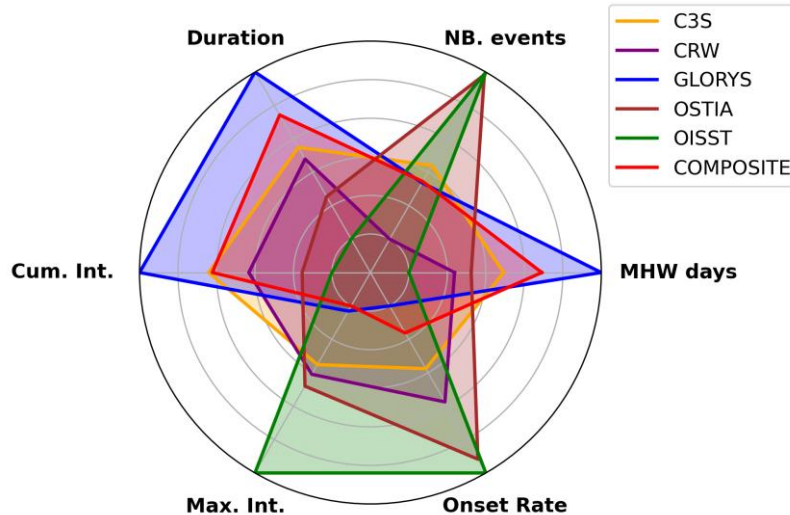


Figure 3: The radar chart is a comparison of all product metrics. The average of MHW metrics are computed for all events detected in the tropical Pacific over 1993-2021 for each product, and normalized by the product that reaches the maximum metric so that all values of the radar chart vary between 0 and 1 (plotted along the radial axes).

The comparison of MHW metrics between products thus highlighted significant differences which vary spatially and between metrics. In the next section, the robustness of the different metrics regarding SST choices is evaluated by quantifying the uncertainty linked to the SST product choice for each metric at both tropical Pacific and regional scales.

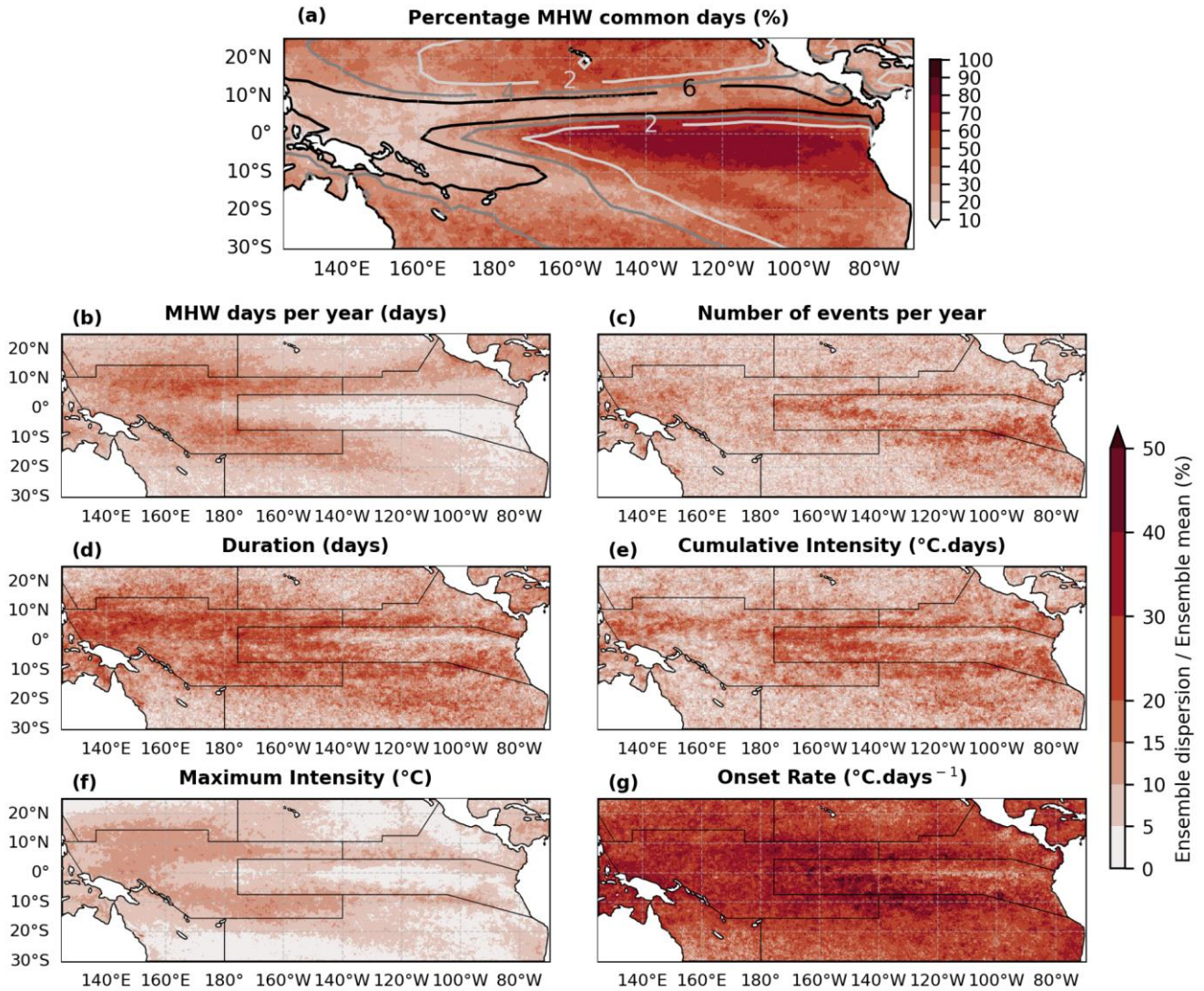
3.3- Uncertainty in MHW metrics due to the SST product choice

3.3.1- Basin-scale overview and regional quantification

The MHW co-occurrence analysis (section 2.3.1) reveals that over the basin, between 10 and 80% of MHW days are detected simultaneously by C3S, CRW, OSTIA, OISST and GLORYS12v1 ~~all six products~~ (Fig. 4a). Excluding the PEQD region, where percentages reach their maximum ranging between 60 and 80%, MHW days in common do not exceed 50% over the tropical Pacific and even drop below 20% in a large part of the basin, in the WARM and PNEC regions. The spatial patterns of common MHW days match well with precipitation contours in the basin (Fig. 4a), with highest common days in area of lowest precipitation in general, an aspect further discussed in section 4.2.

The ensemble dispersion normalized by the ensemble mean for each MHW metric (Fig. 4b-g, section 2.3.1) highlights that the onset rate exhibits the largest normalised dispersion across products ~~is the most sensitive metric to inter-product variability~~.

326 Dispersion for this metric exceeds 30% across much of the tropical Pacific, reaching values above 50% in the southeastern
327 part of the basin (around 10°S-130W, Fig. 4g), where onset rates are small (Fig. 1g). MHW duration also exhibits high
328 sensitivity to the choice of SST product, with normalized dispersion ranging between 20 and 30% over the basin, closely
329 followed by the cumulative intensity and the number of events per year (Fig. 4c,d,e). The MHW days per year and the
330 maximum intensity show the lowest dispersion, with values ranging between less than 5% in the PEQD ~~0-5% (in the PEQD)~~
331 and 20% ~~(30%)~~ in the WARM for the maximum intensity (30% for the total MHW days) (Fig. 4b,f).
332 The high ensemble dispersion values observed in the WARM region across all metrics (Fig. 4b-g) is consistent with the small
333 fraction of MHW days detected simultaneously by all six products in this area (between 10 and 20%, Fig. 4a). The spatial
334 patterns of common MHW days also show good correspondence with dispersion patterns of the total MHW days per year and
335 maximum intensity (Fig. 4b,f), with high dispersion coinciding with a low percentage of common days, and vice versa.



336

337 **Figure 4:** (a) Percentage of MHW days detected simultaneously by C3S, CRW, OSTIA, OISST and GLORYS12v1 ~~the six~~ **SST**
 338 **products** (section 2.3.1), with mean 1993-2021 ERA5 precipitation contours overlaid (temporal average over 1993-2021, in mm/day).
 339 (b-g) Normalized ensemble dispersion for each MHW metric (value in %, section 2.3.1). Black lines indicate regions' limits.
 340

341 The spatial variability of the previous results supports the need of a regional approach in our sensitivity analysis. Consequently,
 342 spatial boxplots of dispersion values within each region are represented in Fig. 5. Across regions, the dispersion distributions
 343 for each metric differ significantly (Mann–Whitney test, $p < 0.05$). The spatial average of dispersion values within each region
 344 is detailed in Fig. 5 (~~exact value~~), providing the uncertainties for each metric and region.

345 The regional analysis (Fig. 5) confirms the basin-scale findings (Fig. 4): the onset rate and duration metrics are the most
 346 sensitive metrics to SST product choice, with uncertainties exceeding 10% of the regional means in all regions and peaking in
 347 the WARM (32.2% for the onset rate, Fig. 5). Cumulative intensity also shows uncertainties larger than 10% in all regions

348 except NPSW and ARC. The number of events per year exceeds 10% uncertainties in three of the seven regions - WARM,
349 PNEC and PEQD (Fig. 5). Finally, the total MHW days per year and maximum intensity are the least impacted metrics with
350 uncertainty lower than 10% in all regions except WARM (and PNEC for MHW days per year).

351 Fig. 5 also highlights the WARM region as the most sensitive region to SST product choice, since percentages of dispersion
352 are higher than 10% whatever the metric chosen. It is closely followed by the PNEC, with uncertainties higher than 10% for
353 all metrics except maximum intensity. Conversely, NPSW and ARC are the regions that exhibit the lowest uncertainties. The
354 PEQD shows some of the lowest dispersion values among all regions for the total MHW days per year and maximum intensity,
355 but for all other metrics dispersion exceeds 10% of the ensemble mean. Moreover, the PEQD shows important dispersion
356 values for dispersion outliers for all metrics with which outliers are two to three times larger than in other regions for the duration
357 and cumulative intensity (reaching 20 days and 35°C.days, respectively, a pattern also observed in SPSG probably due to
358 ENSO induced variability). Outliers distribution is~~The outliers are~~ important as it~~they~~ provides further insights on metrics
359 uncertainties. For example, in PEQD, MHWs detected have an uncertainty of $\pm 0.11^\circ\text{C}$ in maximum intensity with respect to
360 inter-product differences (~~average dispersion value,~~ Fig. 5). However, some dispersion values inside this region can reach
361 more than 0.5°C (Fig. 5), suggesting that MHW analyses inside PEQD should be interpreted with caution if based on a single
362 dataset (almost 1°C of uncertainty for some pixels inside this region).

363

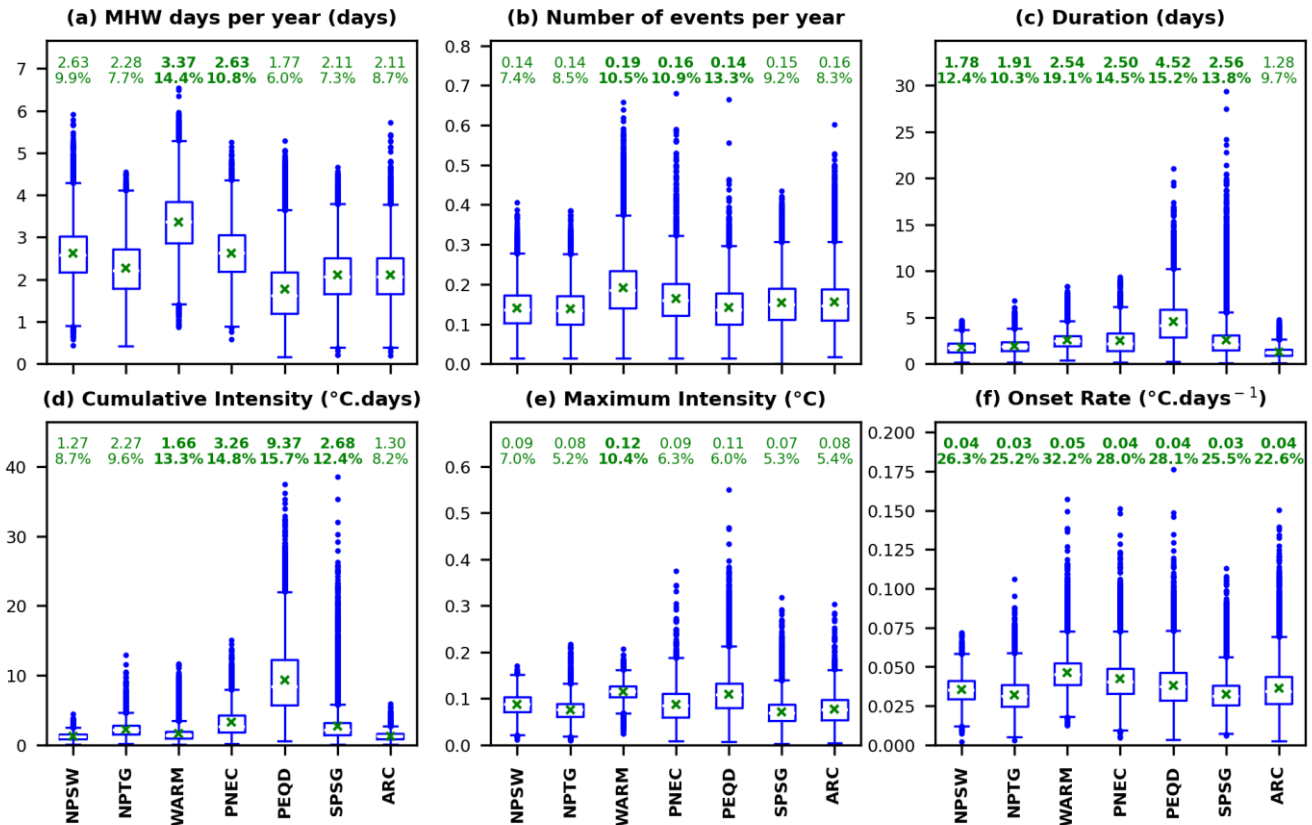


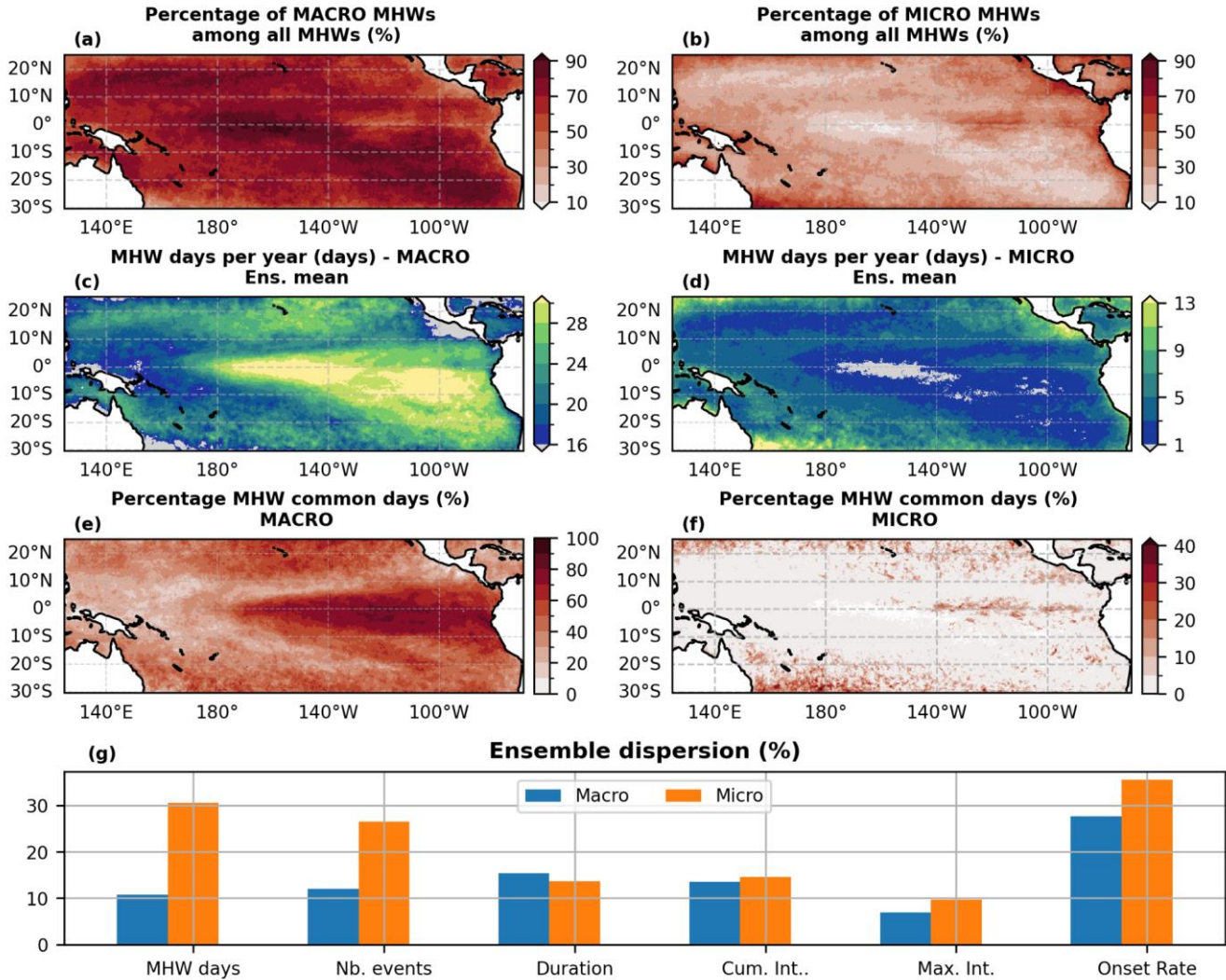
Figure 5: Spatial boxplots of the ensemble dispersion values from Fig. 4b-g for each region. Boxes contain 50% of the values (limits are the first quartile Q1 and third quartile Q3), with the green marker representing the mean value. Whiskers (lines extending from the box) represent the typical range of data; they extend from $Q1 - 1.5 \times (Q3 - Q1)$ to $Q3 + 1.5 \times (Q3 - Q1)$. The dots outside the whiskers are considered as “outliers”. The exact-mean values (green marker) are indicated at the top of each boxplot (1st number from the top), along with its equivalence in percentage of the ensemble mean in the region (2nd number from the top). Mean dispersions higher than 10% of the regional mean value are highlighted in bold.

3.3.2- Metrics uncertainty as a function of MHW size

We now examine whether the metrics sensitivity to the SST product depends on the size of the MHWs. We investigated this hypothesis by filtering MHWs by size (section 2.2.3), and ensemble dispersion was then computed separately for macro and micro-scale events. Spatial patterns of macro ($> 5^\circ \times 5^\circ$) and micro events (Fig. 6a,b,c,d) show that macro events occur mainly in regions influenced by ENSO (PEQD and Ssoutheastern SPSG) while micro events are mainly concentrated near coastlines and at the southern and northern limits of the study area (in the PNEC, WARM, ARC, but also northern NPSW and in SPSG near the shore). Yet, the spatial extent of MHWs at the northern and southern limits of the area of study should be taken with caution for the reasons explained in 2.2.3 (their spatial extent is likely underestimated).

Very few micro-scale MHW days are detected simultaneously by C3S, CRW, OSTIA, OISST and GLORYS12v1 all SST products (Fig. 6f): percentages of MHW common days range between 40% in areas where micro-scale events are numerous

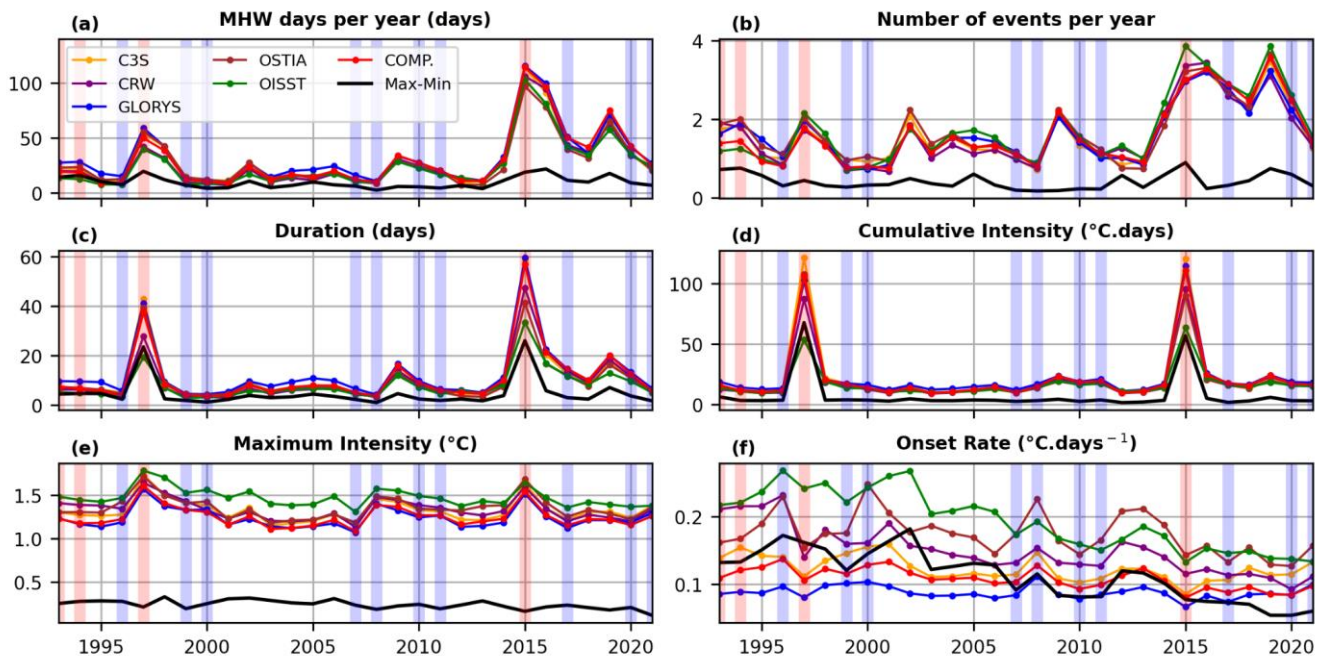
381 and less than 5% where they are fewer. In contrast, percentages of MHW days in common for macro scale events range between
 382 20% in the WARM (where they are fewer) and 80% in the PEQD (Fig. 6e). Differentiating macro and micro-scale events
 383 highlights that dispersion is generally lower for macro-scale events (Fig. 6g). This is particularly striking for the total MHW
 384 days per year and number of events per year, for which ensemble dispersion decreases by more than two between micro- and
 385 macro-scale events when considering (spatial averages over the basin). Dispersion for cumulative intensity, maximum intensity
 386 and onset rate remains slightly lower for macro-scale events compared to micro-scale events, but is slightly higher for duration.



387
 388 **Figure 6:** (a) Percentage of macro-scale MHWs among all events detected over 1993-2021 (i.e. ensemble mean of the total number
 389 of macro events divided by the ensemble mean of the total number of MHWs of all types, multiplied by 100). (b) Same as (a) for
 390 micro-scale MHWs. (c) Ensemble mean of total MHW days per year for macro scale events. (d) Same as (c) for micro-scale MHWs.
 391 (e) Percentage of MHW days detected in common by all six products (section 2.3.1) over 1993-2021 for macro scale events. (f) Same
 392 as (e) for micro-scale MHWs. (g) Spatial average over the tropical Pacific of dispersion values for each metric for macro-scale MHWs
 393 (blue bars) and micro-scale MHWs (orange bars).

394 3.3.3- Temporal variability of the dispersion

395 Having quantified inter-product differences, we investigated their temporal evolution to assess both long-term trends and the
396 influence of ENSO events on their temporal variability. The yearly time series of MHW metrics averaged over the tropical
397 Pacific for each product highlight the inter-annual variability of inter-product differences (black line Fig. 7), which varies
398 appears to vary between metrics. Over the basin, differences between products are rather stable through years for the maximum
399 intensity and onset rate while they seem to increase for years marked by strong El Niño events (1997-98, 2015-16) for the
400 other metrics (Fig. 7). The particularly high values in 2015 compared to 2016 for the metrics duration, cumulative intensity,
401 maximum intensity and rate of onset is explained by the year attribution of MHWs to its time start and the starting of the strong
402 El Niño event in 2015.



403
404 **Figure 7: (a-f) Yearly time series of MHW metrics averaged over the tropical Pacific for each product. Inside each panel, the black**
405 **line represents the largest inter-product difference value for each year (maximum-minimum). The red and blue backgrounds**
406 **indicate years of strong El Niño and La Niña, respectively, according to the Meiv2 index.**
407

408 As Fig. 7 reveals a strong influence of ENSO events on MHW metrics, MHW mean metrics and ensemble dispersion were
409 computed for El Niño MHWs, La Niña MHWs and neutral MHWs as defined in section 2.2.4, in the seven subregions studied
410 (Fig. 8). Our results being similar between MHW days per year and number of events per year as well as between duration
411 and cumulative intensity, only four metrics (MHW days per year, duration, maximum intensity and onset rate) were illustrated
412 in Fig. 8 to make it more readable. Regional maps of MHW mean metrics for the three groups are also shown in Fig. S6 to
413 better understand Fig. 8. Let's note that the method presented here to classify MHWs should be regarded as a first step and
414 does not account for the substantial diversity among ENSO events. In particular, Eastern Pacific and Central Pacific events

(Capotondi et al., 2020) can exert different influences on marine heatwave characteristics (Gregory et al., 2024; Pagli et al., 2025). Our results being similar between MHW days per year and number of events per year as well as between duration and cumulative intensity, only four metrics (MHW days per year, duration, maximum intensity and onset rate) were illustrated in Fig. 8 to make it more readable. Fig. 8a-d highlights that the PNEC and PEQD are highly influenced by El Niño events while the NPSW and ARC are influenced by La Niña events (in these regions, most MHW days per year are attributed to El Niño and La Niña, respectively). Spatial means of ensemble dispersion inside the regions (Fig. 8e-h) highlight that El Niño leads to lower inter-products dispersion in the regions where it has most influence, while it is not the case for La Niña. The decrease in dispersion in regions influenced by El Niño could be due to the presence of macro scale MHWs during El Niño events, which show lower inter-products dispersion as shown in the results of section 3.3.2.

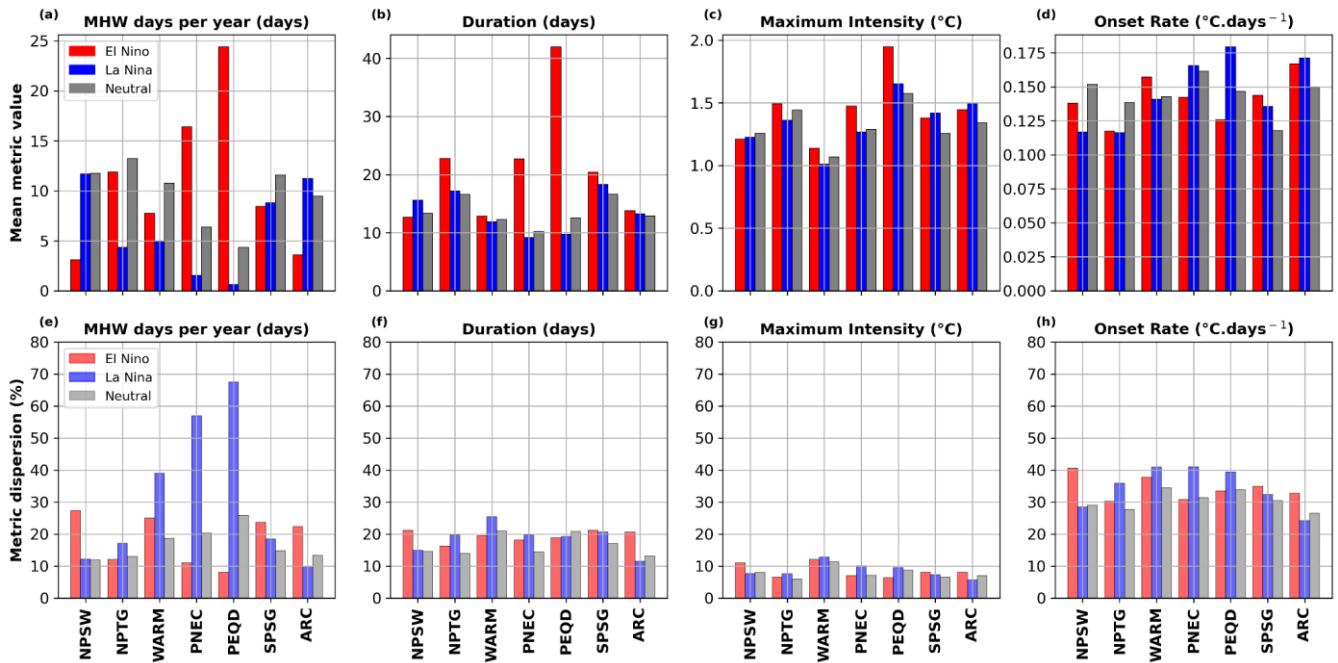


Figure 8: (a-d) Histograms of the spatial means of MHWs metrics (ensemble mean) inside the seven regions of study for the MHW days per year (a), duration (b), maximum intensity (c) and onset rate (d) for El Niño MHWs (red), La Niña MHWs (blue) and neutral (gray). (e-h) Histograms of the spatial mean of ensemble dispersion inside the seven regions of study for the MHW days per year (e), duration (f), maximum intensity (g) and onset rate (h) for El Niño MHWs (red), La Niña MHWs (blue) and neutral (gray).

The yearly time series of the ensemble dispersion and spatial correlation within each region (section 2.3.2, Fig. 9 and Fig. S7) provide more insights on the temporal evolution of inter-product differences, and highlight four main points. First, the ensemble dispersion and ensemble spatial correlation values are coherent: metrics showing the lowest dispersion (maximum intensity and MHW days per year) also exhibit the highest ensemble spatial correlation (values ranging between 0.8 and 1), whereas metrics showing the highest dispersion (onset rate) show the lowest ensemble spatial correlation (values ranging between 0.4 and 0.6). The number of events per year, the duration and the cumulative intensity fall in an intermediate range.

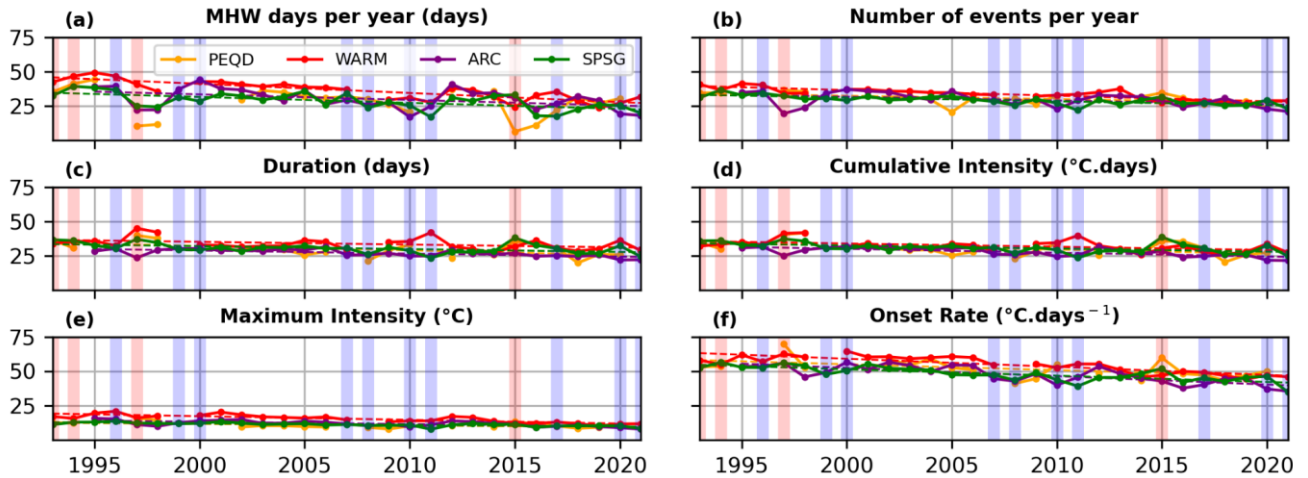
436 The WARM region also shows some of the highest and lowest values of dispersion and spatial correlation, respectively, across
437 all metrics.

438 Second, yearly ensemble dispersion values are higher than those computed on the mean of metrics as in Fig. 4, suggesting
439 ~~since the yearly filter implies more restrictions in MHW comparison. This suggests~~ that ensemble dispersion might be
440 underestimated when it is computed on the mean of metrics over a long period rather than on MHWs yearly metrics.

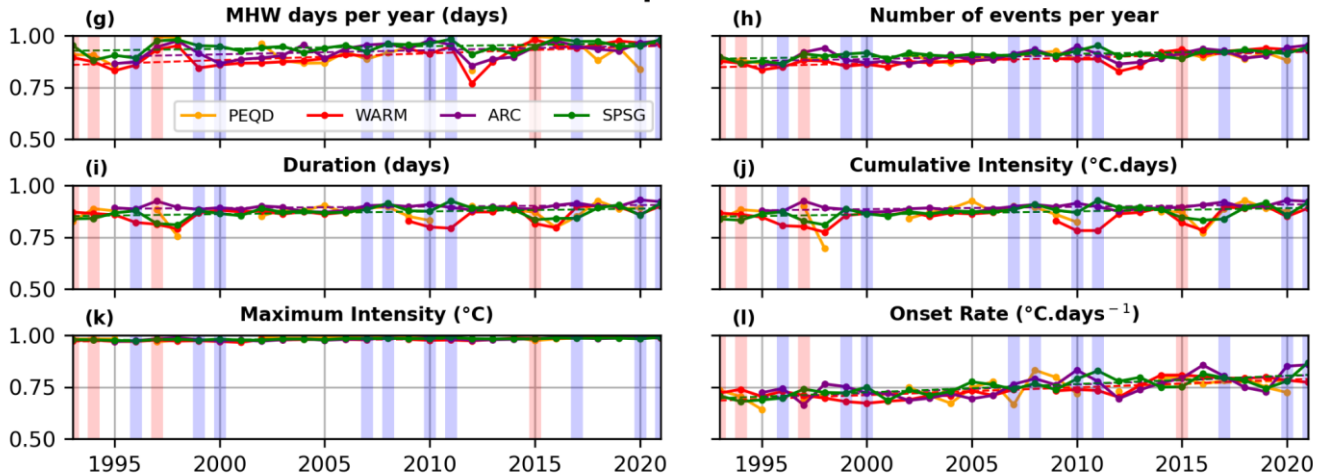
441 Third, the long-term trends suggest a reduction in the inter-product dispersion and an increase in the spatial correlation over
442 the period 1993-2021 for all metrics and regions (Fig. 9 and Fig. S76). In all regions, the largest decreases in ensemble
443 dispersion are observed for the total MHW days per year and the onset rate (-6.6%/dec in WARM and -7.2%/dec in NPSW,
444 respectively, p -values<0.05) while the lowest ones are observed for the maximum intensity (between -1.1%/dec and -
445 2.7%/dec in SPSG and WARM, respectively, p -value<0.05). The highest increasing rates of ensemble spatial correlation are
446 also observed for the total MHW days per year and the onset rate, reached in the WARM and NPSW, respectively.

447 Fourth, ensemble dispersion and spatial correlation show an interannual variability partly linked to ENSO variability. For both
448 statistics, MHW days per year shows the highest interannual variability which is marked by the strong El Niño years of 1997-
449 98 and 2015-16 (minima of dispersion and maxima of spatial correlation). On the contrary, the maximum intensity shows the
450 lowest interannual variability among metrics (Fig. 9 and S7). Yet, the effects of ENSO variability on ensemble dispersion and
451 spatial correlation depend on various factors. They can vary between metrics inside a same region: in the PEQD (where the
452 effects of El Niño ENSO are strong, as shown above), dispersion is clearly lower for strong El Niño years (1997-98, 2015-16)
453 for the total MHW days per year while it is not the case higher for the duration, number of events per year, cumulative intensity
454 and onset rate (dispersion similar or even higher than other years, Fig. 9a-f and also seen in Fig.8 Fig. 9a-f). Similar results are
455 observed in the WARM and SPSG. The effects of ENSO variability can also vary between regions for a same metric: duration
456 shows higher spatial correlations for strong El Niño years in most regions but not in WARM and SPSG where spatial
457 correlation is lower these years and maxima is reached in 2011 (La Niña ~~La Nina~~) in SPSG (Fig. 9i).

Ensemble dispersion (%)



Ensemble spatial correlation



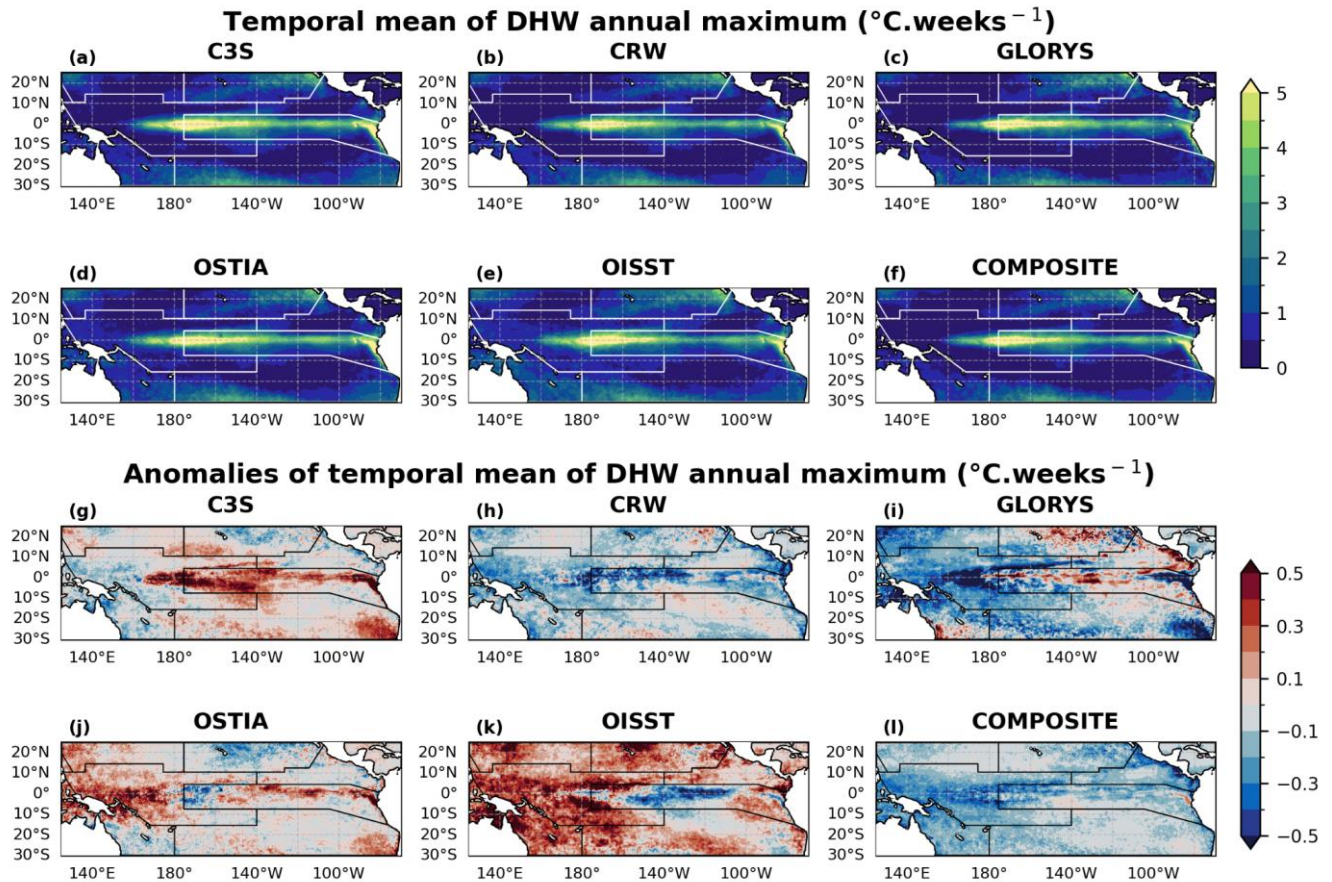
458
459 Figure 9: (a-f) Yearly time series of ensemble dispersion (in percentage) for PEQD, WARM, ARC and SPSG. The dashed lines
460 indicate the significant linear trends (p -value <0.05). The red and blue backgrounds indicate years of strong El Niño and La Niña,
461 respectively, according to the ONI. (g-l) Same as (a-d) for the ensemble spatial correlation (section 2.2.3). Time series in the PNEC,
462 NPTG and NPSW are represented in Supplementary Fig. S76.
463
464

465 ~~Next, we investigate the impact of these SST differences in Once inter-products differences were quantified for MHW~~
466 ~~metrics, they were also analysed for~~ the DHW index, a widely used proxy for coral bleaching.

466 3.4- Uncertainty in the bleaching alerts (Degrees Heating Weeks)

467 The temporal mean of DHW annual maxima over 1993-2021 in the tropical Pacific (Fig. 10a-f) highlights the influence of
468 ENSO on the DHW, with highest values being observed in the central and eastern Equatorial Pacific (more than $5^{\circ}\text{C}\cdot\text{weeks}^{-1}$
469 †) for all products. Such influence is also seen on the yearly time series of DHW annual maximum for each product (Fig. 11a,

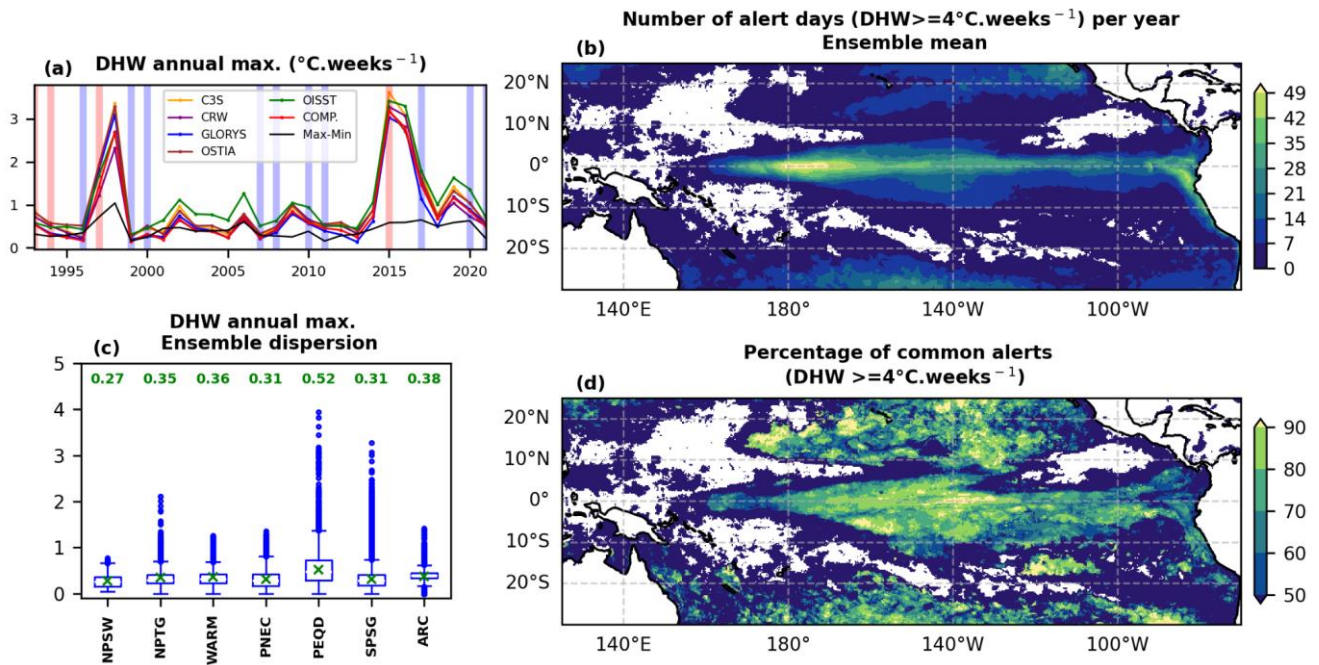
470 spatial average over the tropical Pacific), with maxima observed in strong El Niño years of 1997-98 and 2015-16. Figure 10
 471 highlights significant inter-product differences for DHW annual maximum, with anomalies ranging between $\pm 0.5^{\circ}\text{C}\cdot\text{weeks}^{-1}$
 472 (Fig. 10g-l), and even higher in the western and central eastern equatorial part of the basin. Over the tropical Pacific, the highest
 473 positive anomalies are observed for OISST and C3S while the highest negative anomalies are observed for GLORYS12v1.
 474 Inter-product differences of more than $1^{\circ}\text{C}\cdot\text{weeks}^{-1}$ are observed between C3S and GLORYS12v1 in the PEQD close to the
 475 south American coast (80°W , 0°) and between OISST and GLORYS12v1 in a large area around (140°E , 10°S), between
 476 northern Australia and Indonesia.



477
 478 **Figure 10: (a-f) Temporal mean of DHW annual maximum over the period 1993-2021 for the six SST products. White lines indicate**
 479 **regions' limits.** (g-l) Anomalies of the temporal mean of DHW annual maximum for each product relative to the ensemble mean
 480 (section 2.3.1). **Black lines indicate regions' limits.**

481
 482 Figure 11a confirms that over the years, OISST detects the highest annual maxima of DHW, except in years of strong El Niño
 483 (1997-98, 2015-16) where C3S shows the highest annual DHW maximum (averaged values over the basin). As in Fig. 5,
 484 spatial boxplots of ensemble dispersion in DHW annual maxima within each region are represented in Fig. 11c. Across
 485 regions, the spatial averages of dispersion (green markers and values in Fig. 11c) range between 0.275 and $0.5249^{\circ}\text{C}\cdot\text{weeks}^{-1}$,

486 reached in the NPSW and PEQD, respectively. Such uncertainties, with outliers reaching more than $1^{\circ}\text{C}\cdot\text{weeks}^{-1}$ in all regions
 487 except NPSW, appear critical when comparing DHW values to the bleaching level of alert of $4^{\circ}\text{C}\cdot\text{weeks}^{-1}$ defined by the
 488 NOAA (level 1 alert). This is further illustrated in Fig. 11b,d which show the number of level 1 alerts (ensemble mean) in the
 489 tropical Pacific, and the associated percentage of common alerts between C3S, CRW, OSTIA, OISST and GLORYS12v1
 490 six-products. The spatial average over the basin of the number of level 1 alerts for each product (not shown) revealed that
 491 OISST detected the most alerts closely followed by C3S, while the COMPOSITE detected the fewest, closely followed by
 492 CRW and GLORYS12v1. These results are in line with the maps of anomalies of Figure 10g-l and the previous observations.
 493 In most of the basin, the proportion of level 1 common alerts i.e. the common days for which $\text{DHW} \geq 4^{\circ}\text{C}\cdot\text{weeks}^{-1}$ across
 494 products ranges between less than 50% and 80% (Fig. 11d). In large areas of the basin (in ARC, in PEQD close to the south
 495 American coast and in PNEC), percentages of common alerts reach alerts between all six products reach 70% at maximum.
 496 They even drop lower than 50% south of New Caledonia and in the Coral Sea (ARC). This means that among all bleaching
 497 alert days in these areas (which range between 1 and 2 weeks per year over 1993-2021 for ARC, Fig. 11b), at least one third
 498 or even a half was not detected by at least one of the five products evaluated here. These results confirm that SST product
 499 choice is also crucial to the DHW index.



500
 501 **Figure 11: DHW analysis.** (a) Yearly time-series of DHW annual maxima averaged over the tropical Pacific for each product. The
 502 black line represents the largest inter-product difference value for each year (maximum-minimum). The red and blue backgrounds
 503 indicate years of strong El Niño and La Niña, respectively, according to the ONI Meiv2 index. (b) Ensemble mean of the number of
 504 level 1 alert days ($\text{DHW} \geq 4^{\circ}\text{C}\cdot\text{weeks}^{-1}$) per year, for each pixel of the tropical Pacific over 1993-2021. (c) Spatial boxplot of
 505 ensemble dispersion on DHW annual maxima within the study regions. The green marker represents the mean value, for which the
 506 exact value is indicated on top of the associated boxplot. (d) Percentage of common alerts of level 1 between C3S, CRW, OSTIA,
 507 OISST and GLORYS12v1, among the six SST-products.

508 4- Discussion and conclusions

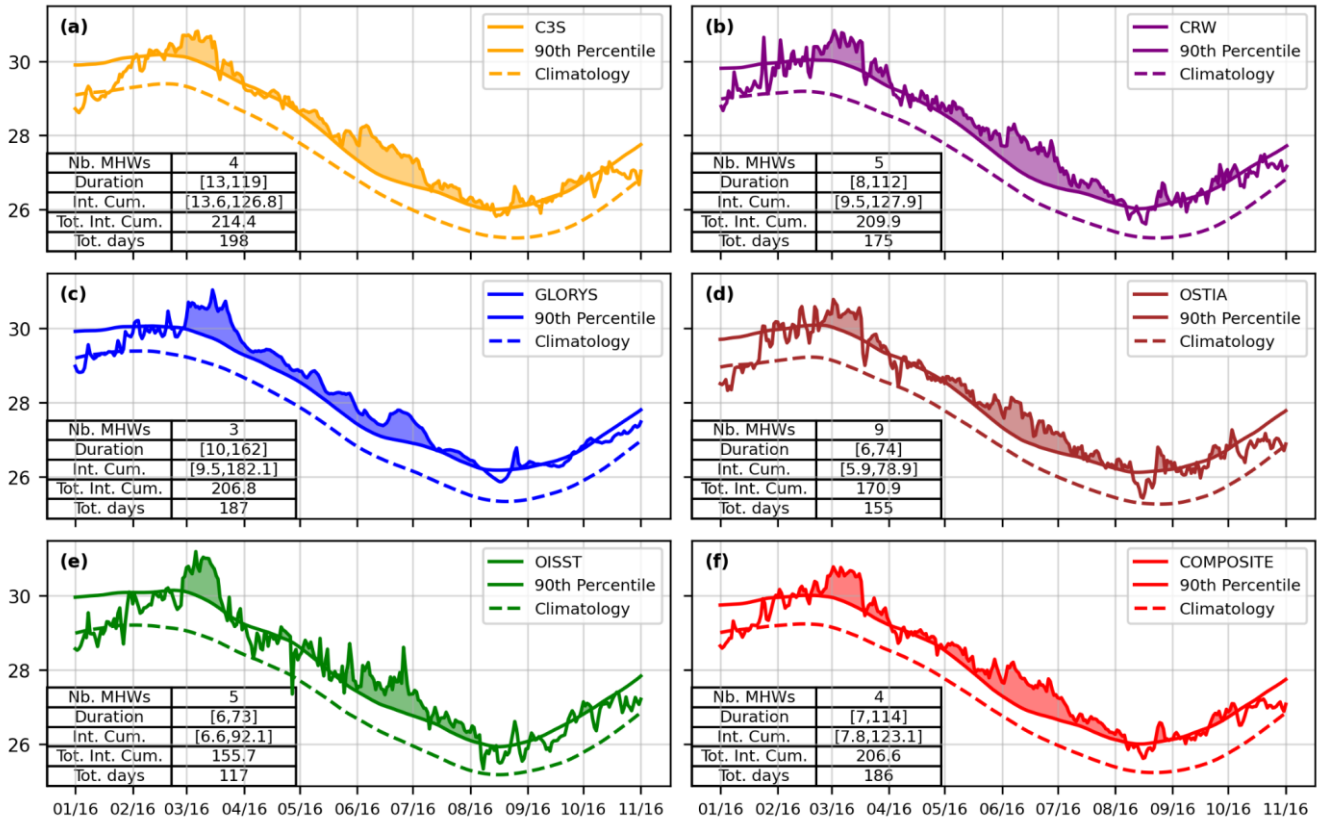
509 In this study, we have quantified the sensitivity of MHW metrics and DHW index to the SST product chosen in the tropical
510 Pacific over 1993-2021, at both basin and regional scales. Uncertainties associated with the choice of the SST product were
511 assessed using ensemble dispersion for each metric and region.

512 4.1- Inter-product differences and uncertainties

513 MHW mean metrics and temporal means of DHW annual maxima show similar spatial patterns in the tropical Pacific across
514 the six SST products evaluated. The observed spatial patterns of MHW metrics are consistent with previous regional (Holbrook
515 et al., 2022; Lal et al., 2025; Pagli et al., 2025) and global MHW studies (Oliver et al., 2021). However, products show
516 significant differences in the absolute values of the mean metrics and DHW index, which can ~~bege~~ up to a factor of two
517 ~~(between OISST and GLORYS12v1)~~. Over the basin, OISST detects the largest maximum intensity, onset rate, number of
518 events and number of bleaching alerts, but the lowest duration, cumulative intensity and number of MHW days per year. On
519 the opposite, the reanalysis GLORYS12v1 shows the largest number of MHW days per year, duration and cumulative intensity
520 along with the lowest onset rate and second lowest maximum intensity, number of events and number of bleaching alerts. Such
521 behaviors for MHW metrics were also observed by Lal et al. (2025) in the South Pacific island countries and by Wang et al.
522 (2024) in the Northwest Pacific. The observed differences between these two products can be notably related to their strong
523 ~~(OISST) and weak (GLORYS12v1) high-frequency (periods shorter than 2 weeks) SST variability~~ ~~_(periods shorter than 2~~
524 ~~weeks) respectively~~ (cf. following section).

525 Inter-product differences can lead to very different interpretations of the same extreme temperature event. As an example, SST
526 time-series from the six products at one location off the eastern Australian Coast (147°E, 13°S) are shown for 2016 ~~(Fig. 12)~~,
527 when a massive MHW occurred across the Southwest Pacific (Dutheil et al., 2024) causing important damage at the Great
528 Barrier Reef (Great Barrier Reef Marine Park Authority report, 2017). The different time series reveal that this MHW was
529 detected by all products (temperatures are above the 90th percentile from approximately February 2016 to September 2016;
530 ~~Fig. 12~~), but in very different ways (Fig. 12). The number of MHW events detected over the time period ranges from 3
531 (GLORYS12v1) to 9 (OSTIA), and the cumulative intensity of the MHWs detected from 78.9°C.days (OSTIA) to
532 182.1°C.days (GLORYS12v1). Consequently, interpretations linked to the biological impacts of such events, (e.g., which
533 metrics have the greatest impact on ecosystems: the number of events? duration? recovery time?) can drastically vary from
534 one SST product to another. Same issue applies to the DHW: for the example of Fig. 12, the level 1 alert for coral bleaching
535 was not reached for C3S (3.34 °C.weeks⁺), and maximum DHW barely reached the alert threshold for GLORYS12v1
536 (4.09°C.weeks⁺) while it largely exceeded it for CRW (5.57°C.weeks⁺). More broadly, the percentage of level 1 bleaching
537 alerts in common ~~between C3S, CRW, OSTIA, OISST and GLORYS12v1 among the six products~~ reaches at maximum ~60-
538 70% in large areas of the tropical Pacific, especially in the ARC and PEQD close to coastal areas, where MHW biological
539 impacts are crucial (Smith et al., 2024). Neo et al. (2023) also showed inconsistency in coral bleaching risk indicators

540 calculated among four temperature datasets (including CRW) between temperature data sources (among four evaluated) in
 541 Northwestern and Southeastern Australia. It is worth noting that DHW values computed here are lower than the
 542 ones from the NOAA CRW daily-global 5km satellite coral bleaching DHW product, probably due to differences in the
 543 MMM climatological baseline (the full period 1993-2021 was used in our study while years 1985-1990 plus 1993 only are
 544 used for CRW DHW product, Heron et al., 2014).



545
 546 **Figure 12: SST time-series of the six products at the same pixel (147E, 13S; off the eastern Australian coast) during the MHW event**
 547 **of 2016. The main MHW characteristics identified over the event period (January 2016 - November 2016) are indicated in the tables**
 548 **at the bottom left of each panel. Values in brackets represent the minimum and maximum duration and cumulative intensity of the**
 549 **detected events.**

550
 551 Regarding metrics sensitivity to the SST product choice, the onset rate is the most affected metric with the highest ensemble
 552 dispersion (between 22.624.2% in the ARC and 323.2% in the WARM) and lowest spatial correlation across all regions of the
 553 tropical Pacific. This metric should therefore be considered very carefully in MHW studies, especially since the onset rate
 554 determines the reaction window to a MHW, a key index for marine decision makers (Spillman et al., 2021). In contrast, the
 555 maximum intensity shows low ensemble dispersion (between 5.25-6% in the NPTG and 10.4% in the WARM) and high
 556 ensemble spatial correlation values in all regions, with a low interannual variability of both parameters in all regions, making
 557 it a robust metric regarding inter-product SST variability. Metrics with intermediate sensitivity - duration, cumulative intensity,

558 number of events per year and number of MHW days per year - should be considered carefully as their ensemble dispersion,
559 spatial correlation and interannual variability show high spatial differences. Consequently, SST product choice, region and
560 study year might all influence these metrics.

561 Our results regarding MHW metrics differ from those of Marin et al. (2021). In their coastal MHW analysis, mean intensity -
562 strongly correlated with maximum intensity - showed the largest inter-product differences among the four datasets considered.
563 This discrepancy may arise from several factors. First, methodological differences: Marin et al. (2021) assessed each product's
564 deviation from the ensemble mean metric using a threshold based on ensemble dispersion to identify outliers and hotspot
565 regions of inter-product differences (pixels with at least one outlier product). Such results depend on the individual product
566 and ensemble mean MHW metrics, whereas our study gives an absolute value of the metric uncertainty by solely focusing on
567 the ensemble dispersion. Second, we studied different types of events in different areas: Marin et al. (2021) focused on coastal
568 MHWs worldwide on detrended SST time series while we studied all MHWs in the tropical Pacific without detrending. ~~Third,~~
569 ~~the SST datasets differ: our ensemble includes both reanalysis and multi-product SST which show higher number of events~~
570 ~~and durations, whereas Marin et al. (2021) used only satellite-derived analyses.~~

571 Despite differences in metric robustness, our sensitivity analysis revealed that ensemble dispersion decreased and spatial
572 correlation increased over time for all metrics and regions, reflecting the growing coherence between satellite SST datasets
573 (Yang et al., 2021) and hence improvements in reanalysis products such as GLORYS12v1 (which assimilates satellite SST
574 data) over the last decades. The intercomparison study of eight global gap-free SST products by Yang et al. (2021) indeed
575 highlighted that global mean SST time series showed larger differences among products during the early period of the satellite
576 era (1982-2002) when there were fewer observations.

577 To estimate an uncertainty in MHW metrics and DHW index, our sensitivity analysis also confirms the need for a regional
578 approach, since ensemble dispersion values and their interannual variability vary across regions and metrics. A summary of
579 uncertainties in each region for the six studied MHW metrics is provided in Fig. 5 and in Fig. 11 for the annual maximum of
580 DHW. Within this regional framework, the WARM region particularly stands out across all MHW metrics, with dispersion
581 values among products higher than 10% of the regional ensemble mean. The SST product considered for MHW analysis should
582 therefore be chosen with caution in this area. ~~-, making SST product choice particularly critical in this area for MHW analysis.~~

583 Regarding DHW, the PEQD particularly stands out with uncertainty reaching $0.5^{\circ}\text{C}\cdot\text{weeks}^{-1}$, which appears crucial when
584 comparing to the level 1 of alert for coral bleaching.

585 ~~Overall, the present inter-product comparison provides scientists uncertainty estimates and informs them about SST~~
586 ~~product limitations regarding the scope of their research.~~

587 **4.2- Potential explanations of these differences**

588 The use of different data sources (satellites with infrared or microwave sensors, geo-stationary or not, use of *in-situ* data or
589 not, and if yes of various types - ships, drifting buoys, moored buoys, Argo), depths of SST estimations (skin layer, foundation),
590 time of SST estimations (dusk to dawn, night-time only, daily mean) and the different data interpolation methods or

591 assimilation methods in the SST products certainly explain the observed inter-product differences (Martin et al., 2012; Dash
592 et al., 2012; Okuro et al. 2014; Fiedler et al., 2019; Huang et al., 2023). The MHW detection and DHW computation methods,
593 both relying on thresholds, then amplifies small differences when computing MHW metrics and DHW.

594 Our results suggest that MHW detection is particularly sensitive to the high frequency variability of the SST signal. The
595 combined analysis of the standard deviation of the high frequency SST signal (filtered at 15 days) in Appendix A (Fig. A1)
596 and the radar chart of Fig. 3 suggest that spiky signals with stronger high frequency variability like OISST and OSTIA detect
597 higher maximum intensity, onset rate and number of events, but lower duration, cumulative intensity and number of MHW
598 days per year. On the opposite, smoother products like GLORYS12v1 or the COMPOSITE with lower high frequency
599 variability (Fig. A1) detect lower maximum intensity, onset rate and number of events, but higher duration, cumulative
600 intensity and number of MHW days per year (Fig. 3). Thus, the similarity of behaviours between GLORYS12v1 and the
601 COMPOSITE (Fig. 3) might reflect the smoothing effect induced by the multi-product mean SST. These effects of high
602 frequency variabilities were also seen in the SST time series of Fig. 12 : climatological levels were similar between products,
603 but OISST and OSTIA signals showed larger high frequency variability (confirmed by Fig. A1), which resulted in the detection
604 of more MHWs of shorter durations (that duration reached 73 and 74 day maximum, respectively, Fig. 12), while
605 GLORYS12v1 or the COMPOSITE showed smoother signals and detected fewer MHWs but of longer durations (duration of
606 maximum 162 days for GLORYS12v1, Fig. 12).

607 It is also worth noting that the sensitivity of MHW metrics to SST high-frequency variability may partly arise from the event
608 definition itself: changing the minimum duration threshold (≥ 5 days) or the maximum gap to consider a continuous event (2
609 days) might affect the inter-product differences. More continuous indices, such as severity (Hobday et al., 2018; Sen Gupta et
610 al., 2020) might help to reduce inter-product differences in MHW diagnostics.

611 A preliminary work on the impact of re-gridding on the observed inter-product differences was also conducted inside two
612 small areas of the tropical Pacific, and results for the area of New Caledonia are presented in Supplementary Information
613 (Table S1 and Fig. S8,S9). The analysis suggests that the re-gridding has little impact on the results of our study but might
614 have an influence on inter-products dispersion for the onset rate metric. C3S and GLORYS also seem to be more impacted by
615 the re-gridding than CRW and OSTIA.

616 The spatial variability of common MHW days ~~appears to be~~ also linked to the spatial scales of MHWs: low (high) percentages
617 of common days correspond to areas with a high proportion of micro (macro) scale events. Indeed, the detection of macro
618 scale MHWs ($> 5^\circ \times 5^\circ$) was shown to be more robust across products compared to micro scale MHWs ($\leq 5^\circ \times 5^\circ$), with
619 percentages of common MHW days for macro events largely higher than for micro events. The high proportions of micro
620 MHWs (Fig. 67b) are also located in the areas of larger high frequency variability (Fig. A1): in the coastal areas of the PNEC,
621 NPTG, ARC, in northern NPSW and along the Equator in the PEQD. Also, the duration, cumulative intensity, maximum
622 intensity and onset rate show slightly higher dispersion values for micro-scale events than for macro-scale ones, but large
623 differences are observed for the total MHW days and number of events per year, for which dispersion is higher by a factor of
624 2 for micro-scale events. Lal et al. (2025) similarly reported strong discrepancies in the number of micro-scale events across

625 products whereas macro-scale events counts were relatively consistent. Consequently, a better understanding of the sensitivity
626 of MHW detection for these spatially small events, as well as an improvement of SST products at these fine scales, might help
627 to reduce the observed inter-product differences.

628 The spatial correspondence between common MHW days across products and climatological precipitation patterns (i.e high
629 precipitation; low percentages of common MHW days and vice versa) suggests that atmospheric conditions in convective areas
630 of the SPCZ and the ITCZ (Brown et al., 2020) influence MHW detection. This effect may be linked to differences in signal
631 retrieval and the handling of outliers in the presence of clouds and convective rainfall (for instance, there are spurious peaks
632 in OISST induced by clouds, Reynolds et al., 2007). Alternatively, the particularly higher dispersion and lower ensemble
633 spatial correlation values in the WARM region could also be explained by the specific MHW characteristics (short, numerous
634 and spatially confined events that are difficult to detect). Nonetheless, the WARM region also shows the strongest decreasing
635 rate in ensemble dispersion over time, suggesting that the growing coherence among satellite SST products in recent years
636 (Yang et al., 2021) might have improved the detection of these short, small spatial scale and weak amplitude events.

637 Regarding the relevance of a multi-product approach, our results highlighted that the COMPOSITE does not show an
638 intermediate “ranking” but rather follows the behaviour of the reanalysis product. Metric estimates from the COMPOSITE
639 were influenced by the smoothing applied when averaging temperature data, which introduced biases in MHW statistics.

640 **4.3- Recommendations**

641 Firstly, our results highlight the importance for MHW scientists to understand the behaviour of the SST product selected in
642 their study, particularly its relative “ranking” compared to other products, which varies according to both the metric and the
643 region considered (section 3.2) but also according to the time period of interest (as magnitude of inter-product differences
644 varies between years, section 3.3.3). The evaluation of the high frequency variability of the SST signal can also give valuable
645 information on the product chosen since it ~~strongly~~ influences MHW detection, as explained in section 4.2. Using several
646 products for robustness is thus essential: because all SST products differ in their construction, we cannot *a priori* argue for a
647 “best” dataset to be used for MHW detection without thorough evaluation against in situ and independent SST dataset. Yet,
648 Fiedler et al., (2019) performed a comparison of SST datasets to *in situ* data and summed up the key strengths and weaknesses
649 of various analyses compared to the others. Beyond characterizing product behaviour, MHW studies should also account for
650 the uncertainty associated with SST product choice when reporting MHW metric estimates. When feasible, the use of several
651 SST datasets can substantially increase the robustness of the results, by defining upper and lower bounds of metric estimates.
652 The same recommendations apply for DHW studies, with other studies underlining the need to compare indicators of thermal
653 stress from different data sets (Neo et al., 2023; Margaritis et al. 2025).

654 It is also worth noting that the sensitivity of MHW metrics to SST high frequency variability may partly arise from the event
655 definition itself: changing the minimum duration threshold (≥ 5 days) or the maximum gap to consider a continuous event (2
656 days) might affect the inter-product differences. More continuous indices, such as severity (Hobday et al., 2018; Sen Gupta et
657 al., 2020) might help to reduce inter-product differences in MHW diagnostics.

658 Our results should also be interpreted carefully at finer scales, such as in coastal areas. Larger differences between satellite
659 SST and in-situ temperature data were observed in coastal regions (Castro et al., 2012; Woo et al., 2020) compared to the
660 overall accuracy of the SST in the global ocean and offshore regions. Woo et al. (2020) identified relationships between errors
661 and coastal zones of vigorous tidal mixing, shallow bathymetry, and absence of microwave measurements. Significant
662 differences between satellite and in-situ data were also observed in atolls and lagoons (Van Wynsberge et al., 2017).

663 ~~Finally, regarding the relevance of a multi-product approach, our results highlight that the COMPOSITE does not show an~~
664 ~~intermediate “ranking” but rather follows the behaviour of the reanalysis product. Metric estimates from the COMPOSITE~~
665 ~~were influenced by the smoothing applied when averaging temperature data, which introduced biases in MHW statistics.~~

666 4.4- Perspectives

667 Our study focuses on the sensitivity of MHW metrics to the choice of the SST product. Yet, other methodological options not
668 investigated in this study can also strongly impact the MHW estimates. Since trends in SST products show differences
669 (Menemenlis et al., 2025), detrending SST time series might influence our results and should be investigated further. Also, as
670 Smith et al. (2025) highlighted the significant influence of the baseline on MHW results, this choice might also impact our
671 conclusions. Choosing other thresholds for MHW detection to focus on the most extreme events (e.g 98th percentile) might
672 also affect the observed inter-product differences. In the same way, other methodologies for characterising MHWs spatial
673 extent (Sun et al. 2023, Pastor et al. 2024) might influence our results. Similar remarks apply to the DHW, for which changing
674 the accumulation window size or anomaly cutoff might impact our results. In addition, the re-gridding of SST datasets onto a
675 common 0.25° grid might also have influenced our results (computing spatial means for re-gridding tends to smooth SST time
676 series), as mentioned in 4.2 and illustrated in Supplementary Table S1 and Fig. S8,S9. Further investigation over the whole
677 area would be needed to thoroughly answer the question of the impact of re-gridding and how much information is lost in the
678 process. -Indeed, computing spatial means for re-gridding tends to smooth SST time series, and might impact MHW detection
679 and DHW computation, as mentioned in 4.2. Further investigation over the whole area would be needed to thoroughly answer
680 the question of the impact of re-gridding and how much information is lost in the process. Also, since Since re-gridding is a
681 common practice in MHW studies, more investigation on the impact of the chosen target resolution could also help to advance
682 MHW research. ~~In the case of SST products intercomparison, Huang et al. (2023) showed that the intercomparison is~~
683 ~~influenced by whether SST products are in their original grids or preprocessed into common coarse grids.~~

684 As in Fiedler et al. (2019) with SST datasets, the comparison of our results to MHW metrics and DHW computed from *in_*
685 *situ* and independent data could add valuable information to the study. Such comparison could help understand how the
686 differences between SST products and *in_situ* SST data are translated through the MHW detection algorithm. However, long
687 time series of in situ data in situ data long allowing enough to allow computation of the climatological background and thus
688 MHWs are very sparse, and the depths of the estimated SST might differ, adding other biases in MHW metrics comparison.
689 Extending our analysis at global scale could also give additional valuable information to users. For DHW computation, the
690 comparison of our results to existing bleaching observations in some focus areas (as done by Neo et al. 2023 in northwestern

691 and southwestern Australian reefs and Margaritis et al. 2025 in the Caribbean) could help to better understand the differences
692 and similarities in bleaching risk indicators across datasets.
693 Including other re-analysis products in addition to GLORYS12v1 in our comparison could also be of interest to better
694 understand the impact of the model and data-assimilation system considered in the different re-analyses on MHW detection,
695 including on their vertical extent. This could be done in the framework of the MER-EP (Marine Environment Reanalysis
696 Evaluation Project), a UN-Decade action led by Mercator-Ocean-International. The comparison of MHW metrics between
697 multiple re-analyses could also benefit from the Observing System Experiments done in the framework of the Synergistic
698 Observing Network for Ocean Prediction (SynObs) project (Fuji et al., 2024), if daily outputs are provided. Such comparisons
699 could also help to quantify the influence of ocean observation systems on MHW metrics estimates.

700

701 In conclusion, this study reveals significant dispersion in key MHW metrics and provides new information on how
702 the choice of the SST product impacts MHW detection and bleaching indices. This sensitivity should be kept in mind in future
703 research on MHWs and the ecological impact of extreme temperature events, and the use of multiple SST products in such
704 studies should be advocated to increase the robustness of the findings.

705

706

707

708 *Authors contribution*

709 CC, RLG, CM and SC designed the study and wrote the initial manuscript draft. CC performed the analysis presented in this
710 manuscript. Discussions and iterative feedback from all co-authors significantly contributed to the revision of the manuscript.

711

712 *Competing interests*

713 The authors declare that they have no conflict of interest.

714

715 *Acknowledgments*

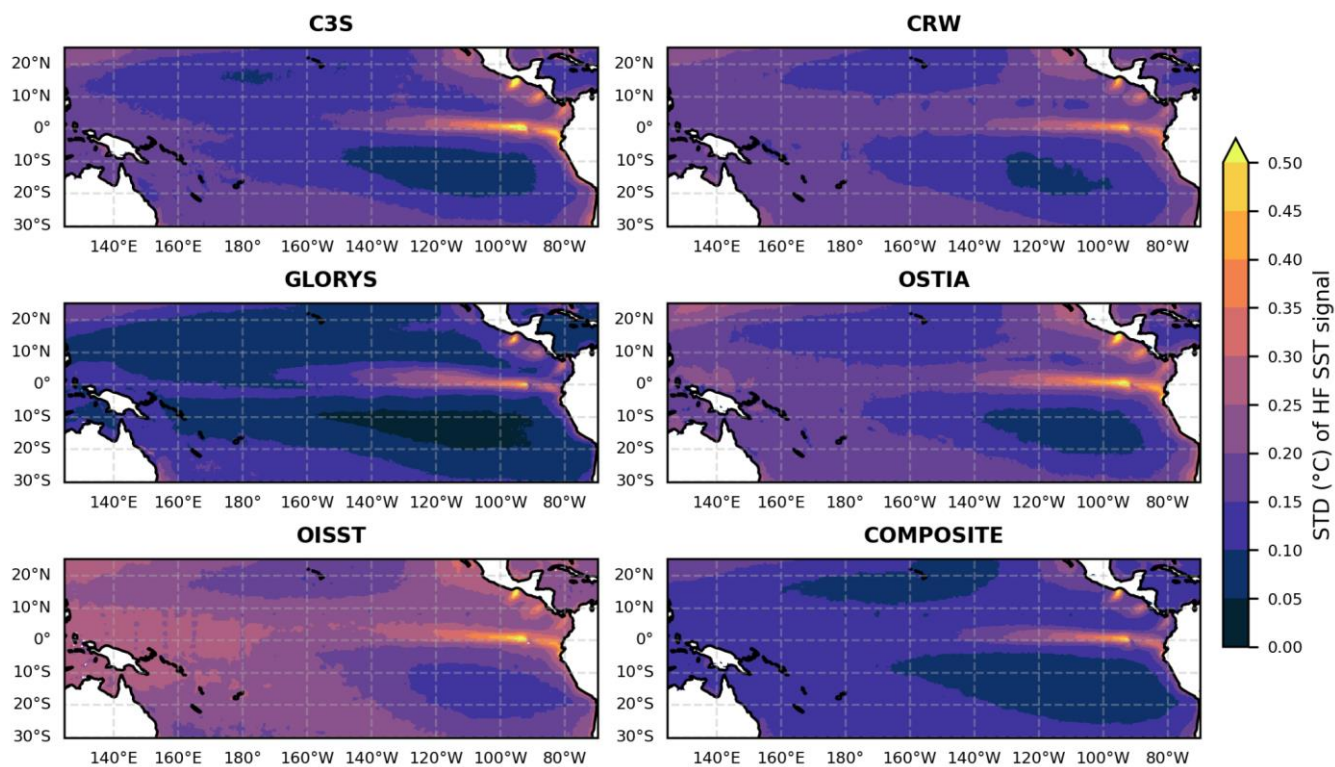
716 We gratefully acknowledge Shilpa Lal for her help and relevant discussions which improved the paper, and Sébastien Petton
717 for his help to parallelize MHW detection code. We also thank colleagues from Mercator-Ocean-International for their advice.
718 The authors also acknowledge the Pôle de Calcul et de Données Marines (PCDM) for providing DATARMOR storage and
719 computational resources (<http://www.ifremer.fr/>). C.C is supported by the Institut français de recherche pour l'exploitation de
720 la mer (IFREMER) through a VSC funding (Volontariat Service Civique) at the Ifremer station of Vairao, Tahiti. The authors
721 acknowledge the support of the French National Research Agency under France 2030 (ANR-23-POCE-0001), as part of the
722 MaHeWa project (grant ANR-23-POCE-0001). This work was also supported by the French national program LEFE (les
723 enveloppes Fluides et l'environnement), project MaheWa-OO.

724

725 *Data Availability Statement*

726 All datasets used in this study are open source and available online. Temperature data from C3S, OSTIA and GLORYS12v1
727 are available on Copernicus :
728 https://data.marine.copernicus.eu/product/SST_GLO_SST_L4_REP_OBSERVATIONS_010_024/description,
729 https://data.marine.copernicus.eu/product/SST_GLO_SST_L4_REP_OBSERVATIONS_010_011/description,
730 https://data.marine.copernicus.eu/product/GLOBAL_MULTIYEAR_PHY_001_030/description, respectively. The CRW data
731 were downloaded from <https://coralreefwatch.noaa.gov/product/5km/index.php> (via ftp). The OISSTv2 data were downloaded
732 from XXX <https://psl.noaa.gov/data/gridded/data.noaa.oisst.v2.highres.html>. All scripts used to obtain the results presented in
733 this study were written in Python and can be shared upon request.

734 **APPENDIX A**



735

736 **Figure A1.** Standard deviation of the high frequency SST signal (high-pass filtered, half-power period of 15 days) over the period 1993-
737 2021 for the six evaluated products.

738 **References**

- 739 Amaya, D. J., Jacox, M. G., Fewings, M. R., Saba, V. S., Stuecker, M. F., Ryzakowski, R. R., Ross, A. C., Stock, C. A.,
740 Capotondi, A., Petrik, C. M., Bograd, S. J., Alexander, M. A., Cheng, W., Hermann, A. J., Kearney, K. A., and Powell, B. S.:
741 Marine heatwaves need clear definitions so coastal communities can adapt, *Nature*, 616, 29–32, doi:10.1038/d41586-023-
742 00924-2, 2023.
- 743
- 744 Andréfouët, S., Dutheil, C., Menkes, C. E., Bador, M., and Lengaigne, M.: Mass mortality events in atoll lagoons:
745 environmental control and increased future vulnerability, *Glob. Change Biol.*, 21, 195–205, doi:10.1111/gcb.12699, 2015.
- 746
- 747 Bian, C., Jing, Z., Wang, H., Wu, L., Chen, Z., Gan, B., and Yang, H.: Oceanic mesoscale eddies as crucial drivers of global
748 marine heatwaves, *Nat. Commun.*, 14, 2970, doi:10.1038/s41467-023-38811-z, 2023.
- 749
- 750 Bonino, G., Masina, S., Galimberti, G., and Moretti, M.: Southern Europe and western Asian marine heatwaves (SEWA-
751 MHWs): A dataset based on macroevents, *Earth Syst. Sci. Data*, 15, 1269–1285. doi:10.5194/essd-15-1269-2023, 2023.
- 752
- 753 Brown, J.R., Lengaigne, M., Lintner, B.R., Widlansky, M.J., van der Wiel, K., Dutheil, C., Linsley, B.B., Matthews, A.J. and
754 Renwick, J.: South Pacific Convergence Zone dynamics, variability and impacts in a changing climate, *Nat. Rev. Earth
755 Environ.*, 1, 530–543, doi:10.1038/s43017-020-0078-2, 2020.
- 756
- 757 [Capotondi, A., Wittenberg, A. T., Kug, J.-S., Takahashi, K., and McPhaden, M. J.: ENSO Diversity, in: El Niño Southern
758 Oscillation in a Changing Climate, American Geophysical Union \(AGU\), 65–86, doi:10.1002/9781119548164.ch4, 2020.](#)
- 759
- 760 Capotondi A., Newman, M., , Xu T., and Di Lorenzo E.: An Optimal precursor of northeast Pacific marine heatwaves and
761 Central Pacific El Niño events, *Geophys. Res. Lett.* 49, e2021GL097350, doi:10.1029/2021GL097350, 2022.
- 762
- 763 Capotondi, A., Rodrigues, R. R., Sen Gupta, A., Benthuisen, J. A., Deser, C., Frölicher, T. L., Lovenduski, N. S., Amaya, D.
764 J., Le Grix, N., Xu, T., Hermes, J., Holbrook, N. J., Martinez-Villalobos, C., Masina, S., Roxy, M. K., Schaeffer, A., Schlegel,
765 R. W., Smith, K. E., and Wang, C.: A global overview of marine heatwaves in a changing climate, *Commun. Earth Environ.*,
766 5, 701, doi:10.1038/s43247-024-01806-9, 2024.
- 767
- 768 Chapman, C.C., Sloyan, B.M., Moore II, Thomas S., Reilly, J. A. and Matear, R.J.: Marine heatwaves in the East Australian
769 current modulated by mesoscale eddies, *J. Geophys. Res. Oceans*, 130, e2024JC021395, doi:10.1029/2024JC021395, 2025.

770 Dash, P., Ignatov, A., Martin, M., Donlon, C., Brasnett, B., Reynolds, R.W., Banzon, V., Beggs, H., Cayula, J.-F., Chao, Y.,
771 Grumbine, R., Maturi, E., Harris, A., Mittaz, J., Sapper, J., Chin, T.M., Vazquez-Cuervo, J., Armstrong, E.M., Gentemann, C.,
772 Cummings, J., Piollé, J.-F., Autret, E., Roberts-Jones, J., Ishizaki, S., Høyer, J.L., and Poulter, D.: Group for High Resolution
773 Sea Surface Temperature (GHRSSST) analysis fields inter-comparisons—Part 2: Near real time web-based level 4 SST Quality
774 Monitor (L4-SQUAM), *Deep Sea Res. Part II: Top. Stud. Oceanogr.*, 77–80, 31-43, doi:10.1016/j.dsr2.2012.04.002, 2012.
775
776 Castro, S. L., Wick, G.A., and Emery, W.J.: Evaluation of the relative performance of sea surface temperature measurements
777 from different types of drifting and moored buoys using satellite-derived reference products, *J. Geophys. Res.*, 117, C02029,
778 doi:10.1029/2011JC007472, 2012.
779
780 Dee, D. P., Uppala, S. M., Simmons, A. J., Berrisford, P., Poli, P., Kobayashi, S., Andrae, U., Balmaseda, M. A., Balsamo, G.,
781 Bauer, P., Bechtold, P., Beljaars, A. C. M., Van De Berg, L., Bidlot, J., Bormann, N., Delsol, C., Dragani, R., Fuentes, M.,
782 Geer, A. J., Haimberger, L., Healy, S. B., Hersbach, H., Hólm, E. V., Isaksen, L., Kållberg, P., Köhler, M., Matricardi, M.,
783 McNally, A. P., Monge-Sanz, B. M., Morcrette, J. -J., Park, B. -K., Peubey, C., De Rosnay, P., Tavolato, C., Thépaut, J. -N.,
784 and Vitart, F.: The ERA-Interim reanalysis: configuration and performance of the data assimilation system, *Q. J. R. Meteorol.*
785 *Soc.*, 137, 553–597, doi:10.1002/qj.828, 2011.
786
787 Donlon, C.J., Martin M., Stark J., Roberts-Jones J., Fiedler E., and Wimmer W.: The Operational Sea Surface Temperature
788 and Sea Ice Analysis (OSTIA) system, *Remote Sens. Environ.*, 116, 140–158, doi:10.1016/j.rse.2010.10.017, 2012.
789
790 Dutheil, C., Lal, S., Lengaigne, M., Cravatte, S., Menkès, C., Receveur, A., Börgel, F., Gröger, M., Houmbreque, F., Le Gendre,
791 R., Mangolte, I., Peltier, A., and Meier, H. E. M.: The massive 2016 marine heatwave in the Southwest Pacific: An “El Niño–
792 Madden-Julian Oscillation” compound event, *Sci. Adv.*, 10, eadp2948, doi:10.1126/sciadv.adp2948, 2024.
793
794 Farchadi, N., McDonnell, L.H., Ryan, S., Lewison, R.L. and Braun, C.D.: Marine heatwaves are in the eye of the beholder,
795 *Nat. Clim. Chang.* 15, 236–239, doi:10.1038/s41558-025-02257-6, 2025.
796
797 Fiedler, K.E., McLaren, A., Banzon, V., Brasnett, B., Ishizaki, S., Kennedy, J., Rayner, N., Roberts-Jones, J., Corlett, G.,
798 Merchant, C.J and Donlon, C.: Intercomparison of long-term sea surface temperature analyses using the GHRSSST Multi-
799 Product Ensemble (GMPE) system, *Remote Sens.*, 222, 18-33, doi:10.1016/j.rse.2018.12.015, 2019.
800
801 Frölicher, T.L., Fischer, E.M. and Gruber, N.: Marine heatwaves under global warming, *Nature*, 560, 360–364,
802 doi:10.1038/s41586-018-0383-9, 2018.
803

804 Fujii, Y., Remy, E., Balmaseda, M.A., Kido, S., Waters, J., Peterson, K.A., Smith, G.C., Ishikawa, I. and Chikhar, K.: The
805 international multi-system OSEs/OSSEs by the UN Ocean Decade Project SynObs and its early results, *Front. Mar. Sci.*, 11,
806 1476131, doi:10.3389/fmars.2024.1476131, 2024.

807

808 Great Barrier Reef Marine Park Authority 2017, Final report: 2016 coral bleaching event on the Great Barrier Reef, GBRMPA,
809 Townsville.

810 [Gregory, C. H., Artana, C., Lama, S., León-FonFay, D., Sala, J., Xiao, F., Xu, T., Capotondi, A., Martinez-Villalobos, and](#)
811 [Holbrook, N. J.: Global Marine Heatwaves Under Different Flavors of ENSO, *Geophys. Res. Lett.*, 51, e2024GL110399,](#)
812 [doi:0.1029/2024GL110399, 2024.](#)

813

814 Hartog, J. R., Spillman, C. M., Smith, G. and Hobday, A. J. Forecasts of marine heatwaves for marine industries: reducing
815 risk, building resilience and enhancing management responses, *Deep Sea Res. Part II Top. Stud. Oceanogr.*, 209, 105276,
816 doi:10.1016/j.dsr2.2023.105276, 2023.

817

818 Heron, S.F., Liu, G., Eakin, C.M., Skirving, W.J., Muller-Karger, F.E., Vega-Rodriguez, M., De La Cour, J.L., Burgess, T.F.
819 and Strong, A.E.: Climatology development for NOAA Coral Reef Watch's 5-km product suite, NOAA technical report
820 NESDIS , 145, doi:10.7289/V59C6VBS, 2014.

821

822 Hersbach, H., Bell, B., Berrisford, P., Hirahara, S., Horányi, A., Muñoz-Sabater, J., Nicolas, J., Peubey, C., Radu, R., Schepers,
823 D., Simmons, A., Soci, C., Abdalla, S., Abellan, X., Balsamo, G., Bechtold, P., Biavati, G., Bidlot, J., Bonavita, M., De Chiara,
824 G., Dahlgren, P., Dee, D., Diamantakis, M., Dragani, R., Flemming, J., Forbes, R., Fuentes, M., Geer, A., Haimberger, L.,
825 Healy, S., Hogan, R. J., Hólm, E., Janisková, M., Keeley, S., Laloyaux, P., Lopez, P., Lupu, C., Radnoti, G., de Rosnay, P.,
826 Rozum, I., Vamborg, F., Villaume, S., and Thépaut, J.-N.: The ERA5 global reanalysis, *Q. J. R. Meteorol. Soc.*, 146, 1999–
827 2049, doi:10.1002/qj.3803, 2020.

828

829 Hobday, A. J., Alexander, L. V., Perkins, S. E., Smale, D. A., Straub, S. C., Oliver, E. C. J., Benthuisen, J. A., Burrows, M.
830 T., Donat, M. G., Feng, M., Holbrook, N. J., Moore, P. J., Scannell, H. A., Sen Gupta, A., and Wernberg, T.: A hierarchical
831 approach to defining marine heatwaves, *Prog. Oceanogr.*, 141, 227–238, doi:10.1016/j.pocean.2015.12.014, 2016.

832

833 Hobday, A. J., Oliver, E. C. J., Gupta, A. S., Benthuisen, J. A., Burrows, M. T., Donat, M. G., Holbrook, N. J., Moore, P. J.,
834 Thomsen, M. S., Wernberg, T., and Smale, D. A.: Categorizing and Naming MARINE HEATWAVES, *Oceanography*, 31,
835 162–173, doi:10.5670/oceanog.2018.205, 2018.

836

837 Hobday, A.J., Burrows, M.T., Filbee-Dexter, K., Holbrook, N.J., Sen Gupta, A., Smale, D.A., Smith, K.E., Thomsen, M.S.
838 and Wernberg, T.: With the arrival of ~~El Niño~~El Niño, prepare for stronger marine heatwaves, *Nature*, 621, 38–41,
839 doi:10.1038/d41586-023-02730-2, 2023.

840

841 Holbrook, N. J., Scannell, H. A., Sen Gupta, A., Benthuyssen, J. A., Feng, M., Oliver, E. C. J., Alexander, L. V., Burrows, M.
842 T., Donat, M. G., Hobday, A. J., Moore, P. J., Perkins-Kirkpatrick, S. E., Smale, D. A., Straub, S. C., and Wernberg, T.: A
843 global assessment of marine heatwaves and their drivers, *Nat. Commun.*, 10, 2624, doi:10.1038/s41467-019-10206-z, 2019.

844

845 Holbrook, N.J., Sen Gupta, A., Oliver, E.C.J., Hobday, A.J., Benthuyssen, J.A, Scannell, H.A., Smale, D.A. and Wernberg,
846 T.: Keeping pace with marine heatwaves, *Nat. Rev. Earth Environ.*, 1, 482–493, doi:10.1038/s43017-020-0068-4, 2020.

847

848 Holbrook, N. J., Hernaman, V., Koshiha, S., Lako, J., Kajtar, J. B., Amosa, P., and Singh, A.: Impacts of marine heatwaves on
849 tropical western and central Pacific Island nations and their communities, *Glob. Planet. Change*, 208, 103680,
850 doi:10.1016/j.gloplacha.2021.103680, 2022.

851

852 Huang, B., Liu, C., Banzon, V., Freeman, E., Graham, G., Hankins, B., Smith, T., and Zhang, H.-M.: Improvements of the
853 Daily Optimum Interpolation Sea Surface Temperature (DOISST) Version 2.1, *J. Clim.*, 34, 2923–2939, doi:10.1175/JCLI-D-
854 20-0166.1, 2021.

855

856 Huang, B., Yin, X., Carton, J. A., Chen, L., Graham, G., Liu, C., Smith, T., & Zhang, H.: Understanding Differences in Sea
857 Surface Temperature Intercomparisons, *J. Atmos. Oceanic Technol.*, 40(4), 455-473. doi:10.1175/JTECH-D-22-0081.1, 2023.

858

859 Intergovernmental Panel on Climate Change (IPCC), 2001: Appendix 12.3: Pattern Correlation Methods. In: *Climate Change*
860 *2001: The Scientific Basis. Contribution of Working Group I to the Third Assessment Report of the Intergovernmental Panel*
861 *on Climate Change* [Houghton, J.T., Y. Ding, D.J. Griggs, M. Noguer, P.J. van der Linden, X. Dai, K. Maskell, and C.A.
862 Johnson (eds.)]. Cambridge University Press, Cambridge, United Kingdom and New York, NY, USA. Available at:
863 <https://archive.ipcc.ch/ipccreports/tar/wg1/470.htm>

864

865 Kajtar, J.B., Holbrook, N.J., Lyth, A., Hobday, A.J., Mundy, C.N. and Ugalde, S.C.: A stakeholder-guided marine heatwave
866 hazard index for fisheries and aquaculture, *Clim. Change*, 177, 26, doi:10.1007/s10584-024-03684-8, 2024.

867

868 Lal, S., Cravatte, S., Menkes, C., Macdonald, J., LeGendre, R., Mangolte, I., Dutheil, C., Holbrook, N., and Nicol, S.:
869 Characterization of Past Marine Heatwaves around South Pacific Island Countries: What really matters?, *EGUsphere*, 1, 48,
870 doi:10.5194/egusphere-2025-3281, 2025.

871

872 Langlais, C., Lenton, A., Heron, S., Evenhuis, C., Sen Gupta, A., Brown, J.N. and Kuchinke, M.: Coral bleaching pathways
873 under the control of regional temperature variability, *Nature Clim. Change*, 7, 839–844, doi:10.1038/nclimate3399, 2017.

874

875 Lellouche, J.-M., Greiner, E., Bourdallé-Badie, R., Garric, G., Melet, A., Drévillon, M., Bricaud, C., Hamon, M., Le Galloudec,
876 O., Regnier, C., Candela, T., Testut, C.-E., Gasparin, F., Ruggiero, G., Benkiran, M., Drillet, Y., Le Traon, P.-Y., Bourdallé-
877 Badie, R., Garric, G., Melet, A., Drévillon, M., Bricaud, C., Hamon, M., Le Galloudec, O., Regnier, C., Candela, T., Testut,
878 C.-E., Gasparin, F., Ruggiero, G., Benkiran, M., Drillet, Y., and Le Traon, P.-Y.: The Copernicus Global 1/12° Oceanic and
879 Sea Ice GLORYS12 Reanalysis, *Front. Earth Sci.*, 9, 698876, doi:10.3389/feart.2021.698876, 2021.

880

881 Li, J., Roughan, M., and Hemming, M.: Interactions between cold cyclonic eddies and a western boundary current modulate
882 marine heatwaves, *Commun. Earth & Environ.*, 4(1), 1–11. doi:10.1038/s43247-023-01041-8, 2023.

883

884 Longhurst, A. R., Chapter 7 – PROVINCES: THE SECONDARY COMPARTMENTS, in: *Ecological Geography of the Sea*,
885 2nd ed., edited by A. R. Longhurst, Academic Press, Burlington, 103–114, doi:10.1016/B978-012455521-1/50008-5, 2007.

886

887 Madec, G., Bell, M., Benshila, R., Blaker, A., Boudrallé-Badie, R., Bricaud, C., Bruciaferri, D., Carneiro, D., Castrillo, M.,
888 Calvert, D., Chanut, J., Clementi, E., Coward, A., Lavergne, C. de, Dobricic, S., Epicoco, I., Éthé, C., Fiedler, E., Ford, D.,
889 Furner, R., Ganderton, J., Graham, T., Harle, J., Hutchinson, K., Iovino, D., King, R., Lea, D., Levy, C., Lovato, T.,
890 Maisonnave, E., Mak, J., Sanchez, J. M. C., Martin, M., Martin, N., Martins, D., Masson, S., Mathiot, P., Mele, F., Mocavero,
891 S., Moulin, A., Müller, S., Nurser, G., Oddo, P., Paronuzzi, S., Paul, J., Peltier, M., Person, R., Rousset, C., Rynders, S.,
892 Samson, G., Schroeder, D., Storkey, D., Storto, A., Téchené, S., Vancoppenolle, M., and Wilson, C.: NEMO Ocean Engine
893 Reference Manual, doi:10.5281/zenodo.14515373, 2024.

894

895 Madden, R. A., and Julian, P.R.: Detection of a 40–50 day oscillation in the zonal wind in the tropical Pacific, *J. Atmos. Sci.*,
896 28, 702–708, doi:10.1175/1520-0469, 1971.

897

898 Madden, R. A., and Julian, P.R.: Description of global-scale circulation cells in the tropics with a 40–50 day period, *J. Atmos.*
899 *Sci.*, 29, 1109–1123, doi:10.1175/1520-0469, 1972.

900

901 Margaritis, G., Kent, E.C. and Foster, G.L.: Intercomparison of satellite-derived SST with logger data in the Caribbean—
902 Implications for coral reef monitoring, *PLOS Climate* 4(1): e0000480, doi:10.1371/journal.pclm.0000480, 2025.

903

904 Marin M., Feng, M., Phillips, H.E. and Bindoff, N.L.: A Global, Multiproduct Analysis of Coastal Marine Heatwaves:
905 Distribution, Characteristics, and Long-Term Trends, *JGR oceans*, 126, 2, doi:10.1029/2020JC016708, 2021.
906

907 Martin, M., Dash, P., Ignatov, A., Banzon, V., Beggs, H., Brasnett, B., Cayula, J.-F., Cummings, J., Donlon, C., Gentemann,
908 C., Grumbine, R., Ishizaki, S., Maturi, E., Reynolds, R. W. and Roberts-Jones, J.: Group for High Resolution Sea Surface
909 Temperature (GHRSSST) analysis fields inter-comparisons. Part 1: A GHRSSST multi-product ensemble (GMPE), *Deep Sea*
910 *Res. Part II: Top. Stud. Oceanogr.*, 77–80, 21–30, doi:10.1016/j.dsr2.2012.04.013, 2012.
911

912 Menemenlis, S., Vecchi, G.A., Yang, W., Fueglistaler, S. and Raghuraman, S.P.: Consequential differences in satellite-era sea
913 surface temperature trends across datasets, *Nat. Clim. Chang.*, 15, 897–903, doi:10.1038/s41558-025-02362-6, 2025.
914

915 Merchant, C.J., Allan, R.P. and Embury, O.: Quantifying the acceleration of multidecadal global sea surface warming driven
916 by Earth’s energy imbalance, *Environ. Res. Lett.*, 20, 024037, doi:10.1088/1748-9326/adaa8a, 2025.
917

918 Misra, R., Sérazin, G., Meissner, K. J. and Gupta, A.S.: Projected changes to Australian marine heatwaves, *Geophys. Res.*
919 *Let.*, 48, e2020GL091323, doi:10.1029/2020GL091323, 2021.
920

921 Neo, V. H. F., Zinke, J., Fung, T., Merchant, C. J., Zawada, K. J. A., Krawczyk, H., and Maina, J. M.: Inconsistent coral
922 bleaching risk indicators between temperature data sources, *Earth and Space Science*, 10, e2022EA002688.
923 doi:10.1029/2022EA002688, 2023.
924

925 Okuro, A., Kubota, M., Tomita, H., and Hihara, T.: Inter-comparison of various global sea surface temperature products, *Int.*
926 *J. Remote Sens.*, 35(14), 5394-5410, doi:10.1080/01431161.2014.926415, 2014.
927

928 Oliver E.C.J., Burrows M.T., Donat M.G., Sen Gupta A., Alexander L.V., Perkins-Kirkpatrick S.E., Benthuisen J.A., Hobday
929 A.J., Holbrook N.J., Moore P.J., Thomsen M.S., Wernberg T. and Smale D.A.: Projected Marine Heatwaves in the 21st Century
930 and the Potential for Ecological Impact, *Front. Mar. Sci.*, 6, 734, doi:10.3389/fmars.2019.00734, 2019.
931

932 Oliver, E. C. J., Benthuisen, J. A., Darmaraki, S., Donat, M. G., Hobday, A. J., Holbrook, N. J., Schlegel, R. W., and Gupta,
933 A. S.: Marine Heatwaves, *Annu. Rev. Mar. Sci.*, 13, 313–342, doi:10.1146/annurev-marine-032720-095144, 2021.
934

935 Pagli, B., Izumo, T., Barboni, A., Chevillard, C., Dutheil, C., Legrand, R., Menkes, C., Rocuet, C., and Cravatte, S.: Marine
936 Heatwaves across the central South Pacific: characteristics, mechanisms, and modulation by the El Niño Southern Oscillation,
937 *EGUsphere [preprint]*, doi:10.5194/egusphere-2025-4166, 2025.

938

939 Pastor, F., Paredes-Fortuny, L. and Khodayar, S.: Mediterranean marine heatwaves intensify in the presence of concurrent
940 atmospheric heatwaves. *Commun Earth Environ* **5**, 797, doi.org/10.1038/s43247-024-01982-8, 2024.

941

942 Pearce, A., Lenanton, R., Jackson, G., Moore, J., Feng, M. and Gaughan, D.: The “marine heat wave” off Western Australia
943 during the summer of 2010/11, Fisheries Research Report No. 222, Department of Fisheries, Western Australia. 40pp., 2011.

944

945 Reynolds, R. W., Smith, T. M., Liu, C., Chelton, D.B., Casey, K.S. and Schlax, M.G.: Daily High-Resolution-Blended
946 Analyses for Sea Surface Temperature, *J. Climate*, **20**, 5473–5496, doi:10.1175/2007JCLI1824.1, 2007.

947

948 Schulzweida, U., CDO User Guide (2.3.0), Zenodo, doi:10.5281/zenodo.10020800, 2023.

949

950 Sen Gupta, A., Thomsen, M., Benthuyesen, J. A., Hobday, A. J., Oliver, E., Alexander, L. V., Burrows, M. T., Donat, M. G.,
951 Feng, M., Holbrook, N. J., Perkins-Kirkpatrick, S., Moore, P. J., Rodrigues, R. R., Scannell, H. A., Taschetto, A. S.,
952 Ummenhofer, C. C., Wernberg, T., and Smale, D. A.: Drivers and impacts of the most extreme marine heatwave events, *Sci.*
953 *Rep.*, **10**, 19359, doi:10.1038/s41598-020-75445-3, 2020.

954

955 Skirving, W., Marsh, B., De La Cour, J., Liu, G., Harris, A., Maturi, E., Geiger, E., and Eakin, C. M.: CoralTemp and the Coral
956 Reef Watch Coral Bleaching Heat Stress Product Suite Version 3.1, *Remote Sens.*, **12**, 3856, doi:10.3390/rs12233856, 2020.

957

958 Smith, K. E., Burrows, M. T., Hobday, A. J., Sen Gupta, A., Moore, P. J., Thomsen, M., Wernberg, T., and Smale, D. A.:
959 Socioeconomic impacts of marine heatwaves: Global issues and opportunities, *Science*, **374**(6566), eabj3593,
960 doi:10.1126/science.abj3593, 2021.

961

962 Smith, K.E., Aubin, M., Burrows, M.T., Filbee-Dexter, K., Hobday, A.J., Holbrook, N.J., King, N.G., Moore, P.J., Sen Gupta,
963 A., Thomsen, M., Wernberg, T., Wilson, E. and Smale, D.A.: Global impacts of marine heatwaves on coastal foundation
964 species, *Nat. Commun.*, **15**, 5052, doi:10.1038/s41467-024-49307-9, 2024.

965

966 Smith, K. E., Sen Gupta, A., Amaya, D., Benthuyesen, J. A., Burrows, M. T., Capotondi, A., Filbee-Dexter, K., Frölicher, T.
967 L., Hobday, A. J., Holbrook, N. J., Malan, N., Moore, P. J., Oliver, E.C. J., Richaud, B., Salcedo-Castro, J., Smale, D. A.,
968 Thomsen, M., and Wernberg, T.: Baseline matters: Challenges and implications of different marine heatwave baselines, *Prog.*
969 *Oceanogr.*, **231**, 103404, doi:10.1016/j.pocean.2024.103404, 2025.

970

971 Spillman C.M., Smith G.A., Hobday A.J. and Hartog J.R.: Onset and Decline Rates of Marine Heatwaves: Global Trends,
972 Seasonal Forecasts and Marine Management, *Front. Clim.*, 3, 801217, doi:10.3389/fclim.2021.801217, 2021.
973

974 Spillman C.M., Hobday, A.J., Behrens, E., Feng, M., Capotondi, A., Cravatte, S., Holbrook, N.J. and Sen Gupta, A.: What
975 makes a marine heatwave forecast useable, useful and used? *Prog. Oceanogr.*, 234, 103464,
976 doi:10.1016/j.pocean.2025.103464, 2025.
977

978 Sun, D., Jing, Z., Li, F. and Wu, L.: Characterizing global marine heatwaves under a spatio-temporal framework. *Prog.*
979 *Oceanogr.* 211, doi:10.1016/j.pocean.2022.102947, 2023.
980

981 Terhaar, J., Burger, F.A., Vogt, L., Frölicher, T.L. and Stocker, T.F.: Record sea surface temperature jump in 2023–2024
982 unlikely but not unexpected, *Nature*, 639, 942–946, doi:10.1038/s41586-025-08674-z, 2025.
983

984 Van Wynsberge, S., Menkes, C., Le Gendre, R., Passfield, T. and Andréfouët, S.: Are Sea Surface Temperature satellite
985 measurements reliable proxies of lagoon temperature in the South Pacific?, *Estuarine, Coastal and Shelf Science*, 199, 117-
986 124, doi:10.1016/j.ecss.2017.09.033, 2017.
987

988 Yang, C., Leonelli, F. E., Marullo, S., Artale, V., Beggs, H., Nardelli, B. B., Chin, T. M., De Toma, V., Good, S., Huang, B.,
989 Merchant, C. J., Sakurai, T., Santoleri, R., Vazquez-Cuervo, J., Zhang, H., & Pisano, A.: Sea Surface Temperature
990 Intercomparison in the Framework of the Copernicus Climate Change Service (C3S), *J. Climate*, 34(13), 5257-5283.
991 doi:10.1175/JCLI-D-20-0793.1, 2021.
992

993 Wang, H., Lu, Y., Zhai, L., Chen, X. and Liu, S.: Variations of surface marine heatwaves in the Northwest Pacific during
994 1993–2019, *Front. Mar. Sci.*, 11, 1323702, doi:10.3389/fmars.2024.1323702, 2024.
995

996 Woo, H.-J., and Park, K.-A.: Inter-Comparisons of Daily Sea Surface Temperatures and In-Situ Temperatures in the Coastal
997 Regions. *Remote Sens.*, 12(10), 1592, doi:10.3390/rs12101592, 2020.